J. Fluid Mech. (2012), *vol.* 706, *pp.* 431–469.
doi:10.1017/jfm.2012.262

Spectral broadening and flow randomization in free shear layers

Xuesong Wu[1,2]† **and Feng Tian**[1]

[1] Department of Mechanics, Tianjin University, Tianjin 300072, PR China

[2] Department of Mathematics, Imperial College London 180 Queen's Gate, London SW7 2AZ, UK

(Received 16 January 2012; revised 16 April 2012; accepted 30 May 2012;
first published online 6 July 2012)

It has been observed experimentally that when a free shear layer is perturbed by a disturbance consisting of two waves with frequencies ω_0 and ω_1, components with the combination frequencies $(m\omega_0 \pm n\omega_1)$ (m and n being integers) develop to a significant level thereby causing flow randomization. This spectral broadening process is investigated theoretically for the case where the frequency difference $(\omega_0 - \omega_1)$ is small, so that the perturbation can be treated as a modulated wavetrain. A nonlinear evolution system governing the spectral dynamics is derived by using the non-equilibrium nonlinear critical layer approach. The formulation provides an appropriate mathematical description of the physical concepts of sideband instability and amplitude–phase modulation, which were suggested by experimentalists. Numerical solutions of the nonlinear evolution system indicate that the present theory captures measurements and observations rather well.

Key words: nonlinear instability, parametric instability, transistion to turbulence

1. Introduction

Free shear layers such as mixing layers and wakes exist in many engineering applications as well as in natural environmental flows. The instability of these flows has been studied extensively for many decades as a classical prototype problem for understanding shear-induced transition to turbulence. As well as being of fundamental importance, the instability and the resulting transition are of great practical relevance; they are, for instance, closely related to chemical reactions in combustion chambers and mass/momentum exchange in atmospheric and oceanographic flows.

The velocity profile of a free shear layer possesses an inflectional point, and hence supports essentially inviscid Rayleigh instability waves. The initial stage is predominantly two-dimensional, and the stability characteristics (e.g. growth rate, phase speed and modal shape) are well predicted by the linear stability theory based on the Rayleigh or Orr–Sommerfeld equation (Sato 1956, 1959; Sato & Kuriki 1961; Michalke 1965; Freymuth 1966; Mattingly & Criminale 1972). As a dominant instability wave propagates and amplifies downstream, it rolls up due to nonlinear effects, and forms concentrated spanwise vortices or 'rollers', which represent the most prominent feature of transition (Ho & Huerre 1984). Such roller structures persist even

† Email address for correspondence: x.wu@ic.ac.uk

when the free shear layer has become fully turbulent (Brown & Roshko 1974; Liu 1989).

As is common with open-flow systems, a free shear layer acts as a noise amplifier, which means that its transition to turbulence is greatly affected by external or initial forcing imposed on the flow (Huerre & Monkewitz 1990). By externally exciting disturbances at suitable discrete frequencies in a controlled manner, one may make a detailed study of the ensuing transition process. In many experiments, the disturbance introduced consists of a single frequency ω_0 and the concomitant subharmonic component $\omega_0/2$; the latter is often introduced in mixing layers in order to study vortex pairing (Winant & Browand 1974; Ho & Huerre 1984).

Sato & Kuriki (1961) were probably the first to consider the nonlinear interaction in a planar wake of two spectral components satisfying no harmonic relation. In addition to the dominant naturally occurring mode with a frequency ω_1, another mode of a different frequency, $\omega_0 < \omega_1$, was introduced by acoustic excitation. They found that when the magnitude of the latter is sufficiently large, the mode ω_1 is inhibited. The transition initiated by such two spectral components was investigated experimentally by Sato (1970) and Miksad (1973) for a planar wake and a mixing layer respectively. The measurement of spectral evolution indicated that the mode with a larger amplitude suppresses the one with a smaller amplitude, confirming the 'suppressing effect' found earlier by Sato & Kuriki (1961). Harmonics of each component are generated downstream due to nonlinear self-interactions. The most significant finding is that the mutual interaction generates a component with the difference frequency $\omega_\nu \equiv (\omega_0 - \omega_1)$; this difference mode has an exceptionally large magnitude, and interacts, in turn, with the harmonics to excite components with combination frequencies $(m\omega_0 \pm n\omega_1)$, or $(m\omega_0 + n\omega_\nu)$ $(m, n = 1, 2, \ldots)$. Distinct peaks appear at these frequencies leading to gradual filling in of the spectrum and eventually to flow randomization (Motohashi 1979). The time series reveal that in the early nonlinear stage the disturbance is in the form of a wavetrain whose amplitude and phase are modulated on the (relatively long) time scale ω_ν^{-1}. The fluctuation becomes increasingly irregular further downstream. Further study by Miksad *et al.* (1982) showed that the spectral broadening and the associated energy cascade can be attributed to amplitude and phase modulations. In all these experiments, the frequency difference $(\omega_0 - \omega_1)$ is fairly small, prompting the authors to interpret their findings qualitatively in terms of sideband interaction/instability. A similar mechanism appears to operate in both natural transition and controlled transition initiated by harmonic excitation (Sato & Saito 1975; Miksad, Jones & Powers 1983) because sideband components are always present near to the most amplified mode or to the seeded mode. Measurements of the so-called quadratic transfer function by Ritz *et al.* (1988) suggest that the filling in of the spectrum is mainly caused by three-wave interactions of the sideband type. This gradual, and primarily two-dimensional, randomization process through 'frequency mixing' was once regarded as being different from the abrupt burst of three-dimensional fluctuations characterizing boundary-layer transition (Sato 1970), but Kachanov, Kozlov & Levchenko (1979) observed later that a fairly similar spectral broadening process took place in a Blasius boundary layer, where transition is induced by the viscous Tollmien–Schlichting instability.

The concepts of amplitude–phase modulations and sideband interactions, suggested by experimentalists (Sato & Saito 1975; Miksad *et al.* 1982), are in fact interlinked. They appear to describe, and to some extent explain, key features of transition in free shear layers. There have been a few attempts to put these physical arguments on a mathematical footing. Miksad (1973) tried to model the interaction of two

modes using the classical weakly nonlinear theory, and accordingly proposed two coupled amplitude equations of Landau type. However, the binary interaction cannot represent sideband interactions, which necessarily involve three modes because the interaction between two modes generates the third component. Kim, Khadra & Powers (1980) established an explicit mathematical relation between the amplitudes of sideband components and the temporal amplitude–phase modulations of a carrier wave. Using model amplitude equations for the coupling among sideband components via the low-frequency difference mode of a fixed amplitude, they also discussed the relation between the amplitude–phase modulations and the coefficients in the amplitude equations. The relevance of the model and results to the experimental observations mentioned above is rather indirect. This is because the amplitude equations were proposed on the basis of the classical weakly nonlinear theory, which was formulated for finite Reynolds numbers; it is now realized that this theory is not applicable to unbounded shear flows (Goldstein & Leib 1988; Wu 2004). Mankbadi (1991) investigated the evolution of multiple interacting modes using the integral energy method (Liu 1989), but their frequencies are assumed to satisfy a harmonic relation, and thus the interaction is not of the sideband form. Further more, to derive the amplitude equations using the energy method one has to make a number of approximations, and appeals to physical arguments for their justification. As will be shown in this paper, for free shear layers the evolution system governing the amplitude and phase modulations are much more complex than those given by Kim *et al.* (1980) and Mankbadi (1991).

In order to shed light on the role of low-frequency components in transferring energy to sideband components, Hajj (1997) considered the stability of a hypothetical unsteady mixing layer with the streamwise velocity profile $U(y,t) = (1 + \epsilon e^{i\omega_m t})U(y)$, where y and t stand for the transverse coordinate and the time variable respectively, and ω_m and ϵ are the modulation frequency and amplitude. Since the base flow is time-periodic, the stability problem is in general governed by a parametrically excited system. However, for the chosen profile of variable separation form, a suitable transformation of the time variable reduces the stability equation to the standard one for a steady flow $U(y)$. The amplitude and phase of the instability mode are modulated on the time scale ω_m^{-1}, and accordingly sideband components appear in the spectrum. While the model was able to capture qualitatively one aspect of the spectral broadening in free shear layers, it is rather *ad hoc* because (*a*) the assumed profile is completely artificial, and (*b*) in experiments low-frequency components are continually generated by interactions of sideband components and evolving, as opposed to having a prescribed amplitude.

In the present paper, we undertake to develop a theoretical description of the above observations, and to put the related physical concepts of sideband instability and amplitude–phase modulation into an appropriate mathematical form. The problem concerned involves nonlinear interactions of multiple instability modes on a spatially developing shear flow. A multitude of competing factors, such as nonlinearity, viscosity and non-equilibrium, operate. In order to account for their effects in a systematic manner, a high-Reynolds-number asymptotic approach has been developed, leading to the nonlinear non-equilibrium critical layer theory; for reviews see Cowley & Wu (1994) and Goldstein (1994). This approach was based on the crucial observation that as a small-amplitude instability mode propagates downstream, its linear growth rate diminishes due to the gradual spreading of the shear layer, and a critical layer emerges in the vicinity of the transverse location where the mean velocity $\bar{U}$ equals the phase speed of the instability mode. Dominant nonlinear interactions first

become significant in this layer, causing the instability wave to evolve nonlinearly, while the non-equilibrium effect associated with the slow growth of the mode also appears at leading order. The resulting nonlinear evolution equations may take different forms depending on the nature of the instability mode(s) under consideration (Cowley & Wu 1994; Sparks & Wu 2008). For a two-dimensional Rayleigh instability mode of a given frequency, the evolution is governed by an amplitude equation coupled with an equation for the vorticity in the critical layer (Goldstein & Hultgren 1988; Goldstein & Leib 1988). An important feature is that the evolution is strongly nonlinear, and as a result all harmonics appear simultaneously at the same order and an initially sinusoidal disturbance rolls up as observed in experiments. The predicted amplitude development was found to be in good quantitative agreement with experiments (Hultgren 1992).

Since the frequencies of the two modes involved in spectral broadening differ by a small amount, they may be viewed as within the sideband of a main carrier wave. The disturbance may thus be represented by a wavetrain with an envelope function that depends on a suitable slow time variable and a slow streamwise variable. The formulation and ensuing analysis involve extending the work of Goldstein & Leib (1988) and Goldstein & Hultgren (1988) to a wavetrain that is modulated in both space and time.

The present work is also motivated by the relevance of wavepackets of instability modes to sound generation in subsonic jets. Such a wavepacket radiates little sound directly, but the spatially and temporally modulated mean-flow distortion, generated by the self-interaction of the wavepacket, acts as a non-compact source to emit low-frequency sound (Wu & Huerre 2009). In the simple case of two waves, the emission is from the nonlinearly generated beating component with the difference frequency. This was demonstrated by Sandham, Morfey & Hu (2006) and Suponitsky, Sandham & Morfey (2010), who used the acoustic analogy and compressible DNS respectively to obtain the acoustic far field. A first-principles theoretical description was given by Wu & Huerre (2009) for a wavepacket of a pair of interacting helical modes, in which case a weakly nonlinear critical layer theory is appropriate. The present work forms a prerequisite for ultimately formulating a first-principles theory for acoustic radiation of a wavepacket of axisymmetric or planar modes, for which the strongly nonlinear critical layer theory is required.

The paper is organized as follows. The problem is formulated in § 2, where appropriate scalings are specified. The disturbance in the main part of the flow and within the critical layer are then analysed. Matching the solutions in these two regions leads to the nonlinear evolution system. The initial and boundary conditions are derived in § 3 by considering respectively the linear regime upstream and the far-field asymptote of the vorticity in the critical layer. A single-frequency disturbance undergoing roll-up represents a ‘base state’. Its linear instability to sideband perturbations is analysed in § 4. The linearized evolution problem describing the sideband instability and the fully nonlinear system, subject to the initial condition mimicking the two-frequency excitation in the experiments, are solved numerically for both a mixing layer and a planar wake. The results are presented and interpreted in § 5. A summary and concluding remarks are given in § 6.

2. Formulation

We consider a spatially developing mean shear layer, perturbed by a small-amplitude two-dimensional disturbance. The flow, assumed to be incompressible, is to be

described by Cartesian coordinates (x, y), where x and y are in the streamwise and transverse directions respectively. They are non-dimensionalized by δ^*, the thickness of the shear layer at a typical location, which is taken to be the origin of the coordinate system. The time t, the velocity (u, v) and the pressure p are normalized by δ^*/U_0, U_0 and ρU_0^2 respectively, where U_0 is a reference velocity and ρ is the density of the fluid. The Reynolds number

$$R = U_0\delta^*/\nu, \tag{2.1}$$

where ν is the kinematic viscosity. We assume that $R \gg 1$ in order to present a self-consistent asymptotic description of the nonlinear development of the disturbance.

The velocity field of the shear layer can be written as $\left(\bar{U}(y; x_3), R^{-1}\bar{V}(y; x_3)\right)$, where $x_3 = x/R$ is the variable describing the slow streamwise variation of the base flow. The perturbed flow field may be written as

$$(u, v) = (\bar{U}(y; x_3), R^{-1}\bar{V}(y; x_3)) + (\tilde{u}, \tilde{v}). \tag{2.2}$$

Since the disturbance is two-dimensional, it is convenient to introduce a streamfunction ψ such that $\tilde{u} = \psi_y$ and $\tilde{v} = -\psi_x$. Substitution into the Navier–Stokes equations yields the perturbation equation

$$\left(\frac{\partial}{\partial t} + \bar{U}\frac{\partial}{\partial x}\right)\nabla^2\psi - \bar{U}''\frac{\partial\psi}{\partial x} - \frac{1}{R}\nabla^4\psi = J(\psi, \nabla^2\psi), \tag{2.3}$$

where $J(\xi, \eta)$ is the standard Jacobian operator. We remind the reader that the terms associated with the non-parallel-flow effect, which is negligible to the order of interest for the present study, are dropped for brevity.

Before presenting the formulation for the nonlinear interaction and development of two instability waves, we consider first the case of a single mode, with a frequency ω_0 say. The mode initially follows linear stability theory, amplifies exponentially and becomes neutral at a streamwise position x_n say. The shear-layer thickness at x_n is taken to be the reference length δ^* mentioned earlier. In the vicinity of x_n, the disturbance nearly attains its maximum, and moreover a critical layer emerges, where nonlinear interactions take place first to affect the overall development. Goldstein & Leib (1988) showed that the disturbance enters a nonlinear stage in a region upstream of x_n, corresponding to $x_3 - x_n = O(\epsilon^{1/2})$, where ϵ is a measure of the magnitude of the disturbance. The normalized frequency deviates from the local neutral frequency, $\alpha_0 c$, by $O(\epsilon^{1/2})$, and thus we may write

$$\omega_0 = \alpha_0 c + \epsilon^{1/2} S_0, \tag{2.4}$$

where α_0 and c denote the wavenumber and phase speed of the local neutral mode respectively, and S_0 is a measure of the scaled frequency deviation. The nonlinear evolution may be described by a slow variable

$$\bar{x} = \epsilon^{1/2} c^{-1} x, \tag{2.5}$$

where c is introduced for convenience. The disturbance in the main part of the shear layer may be represented, to leading-order accuracy, as

$$\psi = \epsilon A^{\dagger}(\bar{x})\phi(y)\mathrm{e}^{\mathrm{i}(\alpha_0 x - \omega_0 t)} + \text{c.c.}, \tag{2.6}$$

where $A^{\dagger}(\bar{x})$ and ϕ represent the scaled amplitude and eigenfunction respectively. The critical layer is non-equilibrium, strongly nonlinear and also viscous if the generic

scaling $R = O(\epsilon^{-3/2})$ is taken, and so we write (Goldstein & Hultgren 1988)

$$R^{-1} = \epsilon^{3/2}\lambda, \tag{2.7}$$

where $\lambda = O(1)$ is the Haberman (1972) parameter.

We now turn to the case of two instability waves with frequencies ω_0 and ω_1. If $\omega_1 - \omega_0 = O(\epsilon^{1/2})$, then the corresponding wavenumbers, α_0 and α_1, differ also by $O(\epsilon^{1/2})$, i.e. $\alpha_1 - \alpha_0 = O(\epsilon^{1/2})$. The eigenfunctions are the same to leading order, and the two modes would enter the nonlinear stage and evolve on the scale $\bar{x}$. The streamfunction ψ in the main part of the shear layer is, to leading order, represented by

$$\begin{aligned}\psi &= \epsilon A_0^{\dagger}(\bar{x})\phi(y)\mathrm{e}^{\mathrm{i}(\alpha_0 x-\omega_0 t)} + \epsilon A_1^{\dagger}(\bar{x})\phi(y)\mathrm{e}^{\mathrm{i}(\alpha_1 x-\omega_1 t)} + \text{c.c.}\\ &= \epsilon\left[A_0^{\dagger}(\bar{x})\mathrm{e}^{-\epsilon^{1/2}S_0 t} + A_1^{\dagger}(\bar{x})\mathrm{e}^{\mathrm{i}(\alpha_1-\alpha_0)x-\mathrm{i}(\omega_1-\omega_0)t-\epsilon^{1/2}S_0 t}\right]\mathrm{e}^{\mathrm{i}\alpha_0(x-ct)}\phi(y) + \text{c.c.}\end{aligned} \tag{2.8}$$

Upon introducing the slow time variable τ and the coordinate ζ (which moves with the phase speed of the neutral mode),

$$\tau = \epsilon^{1/2}t, \quad \zeta = x - ct, \tag{2.9}$$

we may rewrite (2.8) as

$$\psi = \epsilon A^{\dagger}(\bar{x},\tau)\phi(y)\mathrm{e}^{\mathrm{i}\alpha_0\zeta} + \text{c.c.} + o(\epsilon), \tag{2.10}$$

which represents a wavetrain or wavepacket with its amplitude $A^{\dagger}(\bar{x},\tau)$ being modulated simultaneously in time and space. This form of disturbance has, in general, a continuous spectrum of sideband components centred at the carrier-wave frequency ω_0, and is thus more general than the two-mode perturbation (2.8) in that the latter may be viewed as a special case with a spectrum that is a linear combination of $\delta(\omega-\omega_0)$ and $\delta(\omega-\omega_1)$, where δ denotes the Dirac delta function.

The analysis leading to the final evolution system is quite similar to that of Goldstein & Leib (1988) and Goldstein & Hultgren (1988), and so we shall only present the main steps, omitting the details involved. The present work extends the nonlinear critical layer analysis to higher order so that the disturbance can be determined up to $O(\epsilon^{1/2})$ accuracy.

2.1. *Outer expansion*

In the main part of the shear layer, the streamfunction ψ has the expansion

$$\psi = \epsilon A^{\dagger}(\bar{x},\tau)\phi_1\mathrm{e}^{\mathrm{i}\alpha\zeta} + \epsilon^{3/2}\sum_{m=1}^{\infty}\phi_2^{(m)}\mathrm{e}^{\mathrm{i}m\alpha\zeta} + \epsilon^2\sum_{m=0}^{\infty}\phi_3^{(m)}\mathrm{e}^{\mathrm{i}m\alpha\zeta} + \text{c.c.} + \cdots. \tag{2.11}$$

Hereafter we write α_0 as α for brevity. The eigenfunction ϕ_1 satisfies the Rayleigh equation and the boundary condition,

$$\mathscr{L}(\alpha)\phi_1 = 0, \quad \phi_1 \to 0 \quad \text{as } y \to \pm\infty, \tag{2.12}$$

where the Rayleigh operator

$$\mathscr{L}(\alpha) = \left(\frac{\partial^2}{\partial y^2} - \alpha^2\right) - \frac{\bar{U}''}{\bar{U}-c}. \tag{2.13}$$

Let y_c denote the critical level, i.e. $\bar{U}(y_c) = c$, and $\hat{\eta} = y - y_c$. As $\hat{\eta} \to 0$, ϕ_1 has the asymptote,

$$\phi_1 \sim 1 + \frac{1}{2}\left(\alpha^2 + \frac{\bar{U}_c'''}{\bar{U}_c'}\right)\hat{\eta}^2 + \frac{1}{12}\frac{\bar{U}_c^{iv}}{\bar{U}_c'}\hat{\eta}^3 + a_1\left[\hat{\eta} + \frac{1}{6}\left(\alpha^2 + \frac{\bar{U}_c'''}{\bar{U}_c'}\right)\hat{\eta}^3\right] + \cdots, \tag{2.14}$$

where a_1 is a constant. Note that we have normalized the eigenfunction such that $\phi_1 = 1$ at $y = y_c$. As $y \to \pm\infty$,

$$\phi_1 \sim c_{\pm\infty}\mathrm{e}^{-\alpha|y|}. \tag{2.15}$$

The constants $c_{\pm\infty}$ and a_1 are determined once ϕ_1 is obtained globally. The function $\phi_2^{(1)}$ is governed by the inhomogeneous Rayleigh equation

$$\left.\begin{aligned} &\mathscr{L}(\alpha)\phi_2^{(1)} = -2\mathrm{i}\alpha c^{-1}\frac{\partial A^\dagger}{\partial \bar{x}}\phi_1 - (\mathrm{i}\alpha)^{-1}\mathscr{D}_0 A^\dagger \frac{\bar{U}''}{(\bar{U}-c)^2}\phi_1, \\ &\phi_2^{(1)} \to 0 \quad \text{as } y \to \pm\infty, \end{aligned}\right\} \tag{2.16}$$

where we have introduced the differential operator

$$\mathscr{D}_0 = \frac{\partial}{\partial \tau} + \frac{\partial}{\partial \bar{x}}. \tag{2.17}$$

As $y \to y_c$,

$$\begin{aligned} \phi_2^{(1)} \sim{}& b_2^{(1)}\left[1 + \frac{1}{2}\left(\alpha^2 + \frac{\bar{U}_c'''}{\bar{U}_c'}\right)\hat{\eta}^2\right] + a_2^{(1)\pm}\left[\hat{\eta} + O(\hat{\eta}^3)\right] + \frac{\mathrm{i}\bar{U}_c'''}{\alpha \bar{U}_c'^2}\mathscr{D}_0 A^\dagger \hat{\eta}\log|\hat{\eta}| \\ &+ \left[-\mathrm{i}\alpha c^{-1}\frac{\partial A^\dagger}{\partial \bar{x}} + \frac{1}{2}\frac{\mathrm{i}\bar{U}_c'''}{\alpha \bar{U}_c'^2}\chi_a \mathscr{D}_0 A^\dagger\right]\hat{\eta}^2 + O(\hat{\eta}^3 \ln \hat{\eta}), \end{aligned} \tag{2.18}$$

where $b_2^{(1)}$ and $a_2^{(1)\pm}$ are functions of $\bar{x}$ and τ, and $\chi_a = a_1 + (1/2)\bar{U}_c^{iv}/\bar{U}_c'''$. The jump $(a_2^{(1)+} - a_2^{(1)-})$ is to be determined by analysing the critical-layer dynamics. For the boundary-value problem (2.16) to have a solution, a solvability condition

$$a_2^{(1)+} - a_2^{(1)-} = -\mathrm{i}\alpha^{-1}J_2 A_\tau^\dagger + \mathrm{i}(2\alpha c^{-1}J_1 - \alpha^{-1}J_2)A_{\bar{x}}^\dagger \tag{2.19}$$

must be satisfied, where

$$J_1 = \int_{-\infty}^{\infty}\phi_1^2\,\mathrm{d}y, \quad J_2 = \int_{-\infty}^{\infty}\frac{\bar{U}''\phi_1^2}{(\bar{U}-c)^2}\,\mathrm{d}y. \tag{2.20}$$

By the standard method of order reduction, the general solution for $y = O(1)$ can be expressed as

$$\phi_2^{(1)} = B^\dagger\phi_1 + C^\pm\mathscr{F}_0 - 2\mathrm{i}\alpha c^{-1}A_{\bar{x}}^\dagger\mathscr{F}_1 - (\mathrm{i}\alpha)^{-1}\mathscr{D}_0 A^\dagger\mathscr{F}_2, \tag{2.21}$$

where $B^\dagger(\bar{x}, \tau)$ is a function of $\bar{x}$ and τ to be determined at the next order, and

$$\mathscr{F}_0 = \phi_1\int_{y_c}^{y}\frac{1}{\phi_1^2}\,\mathrm{d}y, \tag{2.22a}$$

$$\mathscr{F}_1 = \phi_1\int_{y_c}^{y}\frac{1}{\phi_1^2}\,\mathrm{d}\tilde{y}\int_{\infty}^{\tilde{y}}\phi_1^2(\xi)\,\mathrm{d}\xi, \quad \mathscr{F}_2 = \phi_1\int_{y_c}^{y}\frac{1}{\phi_1^2}\,\mathrm{d}\tilde{y}\int_{\infty}^{\tilde{y}}\frac{\bar{U}''\phi_1^2}{(\bar{U}-c)^2}\,\mathrm{d}\xi. \tag{2.22b}$$

In order for $\phi_2^{(1)}$ to satisfy the boundary conditions that $\phi_2^{(1)} \to 0$ as $y \to \pm\infty$, we have to set

$$C^+ = 0, \quad C^- = -2\mathrm{i}\alpha c^{-1} J_1 A_{\bar{x}}^\dagger - (\mathrm{i}\alpha)^{-1} J_2 \mathscr{D}_0 A^\dagger. \tag{2.23}$$

Taking the limit $y \to y_c$ in (2.21) and comparing the result with (2.18), we find that

$$b_2^{(1)} = B^\dagger, \quad a_2^{(1)\pm} = C^\pm + a_1 B^\dagger - 2\mathrm{i}\alpha c^{-1} A_{\bar{x}}^\dagger \int_\infty^{y_c} \phi_1^2 \,\mathrm{d}y - (\mathrm{i}\alpha)^{-1} \mathscr{D}_0 A^\dagger J_0, \tag{2.24}$$

where

$$J_0 = \int_\infty^{\hat{a}} \frac{\bar{U}''\phi_1^2}{(\bar{U}-c)^2}\,\mathrm{d}y + \int_{\hat{a}}^{y_c} \left[\frac{\bar{U}''\phi_1^2}{(\bar{U}-c)^2} - \frac{\bar{U}_c'''}{\bar{U}_c'^2(y-y_c)}\right]\mathrm{d}y - \frac{\bar{U}_c'''}{\bar{U}_c'^2}\ln|\hat{a}-y_c|, \tag{2.25}$$

with $\hat{a} \neq y_c$ an arbitrary constant.

The harmonic components $\phi_2^{(m)}$ satisfy homogeneous Rayleigh equations and boundary conditions

$$\mathscr{L}(m\alpha)\phi_2^{(m)} = 0, \quad \phi_2^{(2)} \to 0 \quad \text{as } y \to \pm\infty \ (m = 2, 3, \ldots), \tag{2.26}$$

and as $\hat{\eta} \to 0$,

$$\phi_2^{(m)} \sim b_2^{(m)} \left\{1 + \frac{1}{2}\left(m^2\alpha^2 + \frac{\bar{U}_c'''}{\bar{U}_c'}\right)\hat{\eta}^2 + \cdots\right\} + a_2^{(m)\pm}\hat{\eta} + O(\hat{\eta}^2). \tag{2.27}$$

It should be noted that despite being governed by homogeneous equations, $\phi_2^{(m)}$ are not eigenfunctions because there is a forcing from the interaction within the critical layer through the jumps $(a_2^{(m)+} - a_2^{(m)-})$, rendering the boundary-value problem inhomogeneous. An important fact of a strong nonlinear critical layer is that all harmonics are generated simultaneously at the same order rather than successively at higher orders as in the classical weakly nonlinear theory.

At $O(\epsilon^2)$, the component with the fundamental frequency, $\phi_3^{(1)}$, satisfies the equation

$$\begin{aligned}\mathscr{L}(\alpha)\phi_3^{(1)} = &-\frac{2\mathrm{i}\alpha}{c}B_{\bar{x}}^\dagger\phi_1 - (\mathrm{i}\alpha)^{-1}\mathscr{D}_0 B^\dagger \frac{\bar{U}''\phi_1}{(\bar{U}-c)^2} - \frac{2\mathrm{i}\alpha}{c}C_{\bar{x}}^\pm\mathscr{F}_0 - (\mathrm{i}\alpha)^{-1}\mathscr{D}_0 C^\pm \frac{\bar{U}''\mathscr{F}_0}{(\bar{U}-c)^2} \\ &- 4\alpha^2 c^{-2} A_{\bar{x}\bar{x}}^\dagger \mathscr{F}_1 + 2c^{-1}\mathscr{D}_0 A_{\bar{x}}^\dagger \left\{\mathscr{F}_2 + \frac{\bar{U}''\mathscr{F}_1}{(\bar{U}-c)^2}\right\} - \alpha^{-2}\mathscr{D}_0^2 A^\dagger \frac{\bar{U}''\mathscr{F}_2}{(\bar{U}-c)^2} \\ &- \frac{1}{c^2}A_{\bar{x}\bar{x}}^\dagger\phi_1 - \alpha^{-2}\mathscr{D}_0^2 A^\dagger \frac{\bar{U}''\phi_1}{(\bar{U}-c)^3} - \alpha^{-2}c^{-1}\mathscr{D}_0 A_{\bar{x}}^\dagger \frac{\bar{U}''\phi_1}{(\bar{U}-c)^2}.\end{aligned} \tag{2.28}$$

As $y \to y_c$,

$$\begin{aligned}\phi_3^{(1)} \sim\ & b_3^{(1)}\left\{1 + \frac{1}{2}\left(\alpha^2 + \frac{\bar{U}_c'''}{\bar{U}_c'}\right)\hat{\eta}^2 + \cdots\right\} + a_3^{(1)\pm}\hat{\eta} + \frac{\bar{U}_c'''}{\alpha^2\bar{U}_c'^3}\mathscr{D}_0 A^\dagger \ln\hat{\eta} \\ &+ \left\{\frac{\mathrm{i}\bar{U}_c'''}{\alpha\bar{U}_c'^2}\mathscr{D}_0 B^\dagger - \frac{\bar{U}_c'''}{\alpha^2\bar{U}_c'^3}\left[\chi_a\mathscr{D}_0^2 A^\dagger + \frac{\bar{U}_c'}{c}\mathscr{D}_0 A_{\bar{x}}^\dagger\right]\right\}\hat{\eta}\ln\hat{\eta} + O(\hat{\eta}^2\ln\hat{\eta}).\end{aligned} \tag{2.29}$$

The solvability of (2.28) yields the equation for $B^\dagger$

$$a_3^{(1)+} - a_3^{(1)-} = -\mathrm{i}\alpha^{-1}J_2\frac{\partial B^\dagger}{\partial \tau} + \mathrm{i}(2\alpha c^{-1}J_1 - \alpha^{-1}J_2)\frac{\partial B^\dagger}{\partial \bar{x}} - \gamma_{11}\frac{\partial^2 A^\dagger}{\partial \bar{x}^2} - \gamma_{12}\frac{\partial^2 A^\dagger}{\partial \tau \partial \bar{x}} - \gamma_{22}\frac{\partial^2 A^\dagger}{\partial \tau^2}, \tag{2.30}$$

where use has been made of (2.24), and we have put

$$\gamma_{11} = -4\alpha^2 c^{-2}(J_1H_1 + I_1) + 2c^{-1}(J_2H_1 + J_1H_2 + I_2 + G_1) - \alpha^{-2}(J_2H_2 + G_2 + J_3 + J_2/c) - c^{-2}J_1, \tag{2.31a}$$

$$\gamma_{12} = 2c^{-1}(J_2H_1 + J_1H_2 + I_2 + G_1) - \alpha^{-2}(2J_2H_2 + 2G_2 + 2J_3 + J_2/c), \tag{2.31b}$$

$$\gamma_{22} = -\alpha^{-2}(J_2H_2 + G_2 + J_3), \tag{2.31c}$$

with

$$I_j = \int_{-\infty}^{\infty}\phi_1\mathscr{F}_j\,\mathrm{d}y, \quad G_j = \int_{-\infty}^{\infty}\frac{\bar{U}''\phi_1\mathscr{F}_j}{(\bar{U}-c)^2}\,\mathrm{d}y \quad (j=1,2), \tag{2.32}$$

$$H_1 = \int_{-\infty}^{y_c}\phi_1\mathscr{F}_0\,\mathrm{d}y, \quad H_2 = \int_{-\infty}^{y_c}\frac{\bar{U}''\phi_1\mathscr{F}_0}{(\bar{U}-c)^2}\,\mathrm{d}y, \quad J_3 = \int_{-\infty}^{\infty}\frac{\bar{U}''\phi_1^2}{(\bar{U}-c)^3}\,\mathrm{d}y. \tag{2.33}$$

2.2. *Inner expansion: critical layer analysis*

The strongly nonlinear critical layer has a width of $O(\epsilon^{1/2})$ (Goldstein & Leib 1988), suggesting the local transverse variable

$$Y = \hat{\eta}/\epsilon^{1/2} = (y - y_c)/\epsilon^{1/2}. \tag{2.34}$$

The streamfunction ψ expands as

$$\psi = \epsilon\Psi_0 + \epsilon^{3/2}\Psi_1 + \epsilon^2\ln\epsilon^{1/2}\Psi_{2L} + \epsilon^2\Psi_2 + \epsilon^{5/2}\Psi_3 + \cdots. \tag{2.35}$$

The first three terms are the straightforward continuation of the outer solution, namely,

$$\left.\begin{aligned}\Psi_0 = A^\dagger\mathrm{e}^{\mathrm{i}\alpha\zeta} + \mathrm{c.c.}, \qquad \Psi_1 = \sum b_2^{(m)}\mathrm{e}^{\mathrm{i}m\alpha\zeta} + a_1A^\dagger Y\mathrm{e}^{\mathrm{i}\alpha\zeta} + \mathrm{c.c.},\\ \Psi_{2L} = \frac{\mathrm{i}\bar{U}_c'''}{\alpha\bar{U}_c'^2}\mathscr{D}_0A^\dagger Y + \mathrm{c.c.},\end{aligned}\right\} \tag{2.36}$$

and it can be easily checked that they satisfy the required equations.

Substituting the expansion (2.35) with (2.36) into (2.3), and making use of (2.5), (2.7), (2.9) and (2.34), we obtain the equation for Ψ_2. That equation can be simplified by introducing

$$\Omega^\dagger = \Psi_{2,YY} - \left(\alpha^2 + \frac{\bar{U}_c'''}{\bar{U}_c'}\right)(A^\dagger\mathrm{e}^{\mathrm{i}\alpha\zeta} + \mathrm{c.c.}). \tag{2.37}$$

It follows then that

$$\mathscr{L}_{\mathscr{N}}\,\Omega^\dagger = -\frac{\bar{U}_c'''}{\bar{U}_c'}(\mathscr{D}_0A^\dagger\mathrm{e}^{\mathrm{i}\alpha\zeta} + \mathrm{c.c.}), \tag{2.38}$$

where the nonlinear operator

$$\mathscr{L}_{\mathscr{N}} = \left(\frac{\partial}{\partial\tau} + \frac{\partial}{\partial\bar{x}} + \bar{U}_c' Y\frac{\partial}{\partial\zeta}\right) - (\mathrm{i}\alpha A^{\dagger}\mathrm{e}^{\mathrm{i}\alpha\zeta} + \mathrm{c.c.})\frac{\partial}{\partial Y} - \lambda\frac{\partial^2}{\partial Y^2}. \tag{2.39}$$

Matching with the outer solution for the fundamental component at $O(\epsilon^{3/2})$ gives the jump $(a_2^{(1)+} - a_2^{(1)-})$, which is inserted into (2.19) to obtain

$$\frac{\alpha}{2\pi}\int_{-\infty}^{\infty}\int_{0}^{2\pi/\alpha} \Omega^{\dagger}\mathrm{e}^{-\mathrm{i}\alpha\zeta}\,\mathrm{d}\zeta\,\mathrm{d}Y = -\mathrm{i}\alpha^{-1}J_2\frac{\partial A^{\dagger}}{\partial\tau} + \mathrm{i}(2\alpha c^{-1}J_1 - \alpha^{-1}J_2)\frac{\partial A^{\dagger}}{\partial\bar{x}}. \tag{2.40}$$

Matching the harmonic components determines the jumps

$$a_2^{(m)+} - a_2^{(m)-} = \frac{\alpha}{2\pi}\int_{-\infty}^{\infty}\int_{0}^{2\pi/\alpha} \Omega^{\dagger}\mathrm{e}^{-\mathrm{i}m\alpha\zeta}\,\mathrm{d}\zeta\,\mathrm{d}Y \quad (m = 2, 3, \ldots). \tag{2.41}$$

Once $\Omega^{\dagger}$ is known, the harmonics in the main part of the shear layer can be obtained by solving (2.26) subject to (2.27) and (2.41).

At $O(\epsilon^{5/2})$, we obtain the equation for Ψ_3

$$\begin{aligned}\mathscr{L}_{\mathscr{N}}\Psi_{3,YY} = {} & \frac{1}{2}\bar{U}_c^{iv}Y^2\Psi_{0,\zeta} + c^{-1}\left[\bar{U}_c'''Y - \bar{U}_c'Y\frac{\partial^2}{\partial\zeta^2} - 2\left(\frac{\partial}{\partial\tau} + \frac{\partial}{\partial\bar{x}} + \bar{U}_c'Y\frac{\partial}{\partial\zeta}\right)\frac{\partial}{\partial\zeta}\right]\Psi_{0,\bar{x}} \\ & - \left(\frac{\partial}{\partial\tau} + \frac{\partial}{\partial\bar{x}} + \bar{U}_c'Y\frac{\partial}{\partial\zeta}\right)\Psi_{1,\zeta\zeta} + \bar{U}_c'''Y\Psi_{1,\zeta} - c^{-1}\bar{U}_c'Y\Psi_{2,YY\bar{x}} \\ & + (\Psi_{1,\zeta} + c^{-1}\Psi_{0,\bar{x}})\Psi_{2,YYY} - \Psi_{1,Y}\Psi_{2,YY\zeta} + \Psi_{0,\zeta}\Psi_{1,Y\zeta\zeta} - \Psi_{1,Y}\Psi_{0,\zeta\zeta\zeta}.\end{aligned} \tag{2.42}$$

Upon introducing $\Omega_3^{\dagger}$ via the substitution

$$\begin{aligned}\Omega_3^{\dagger} = {} & \Psi_{3,YY} - \left\{\left[\frac{1}{2}\frac{\bar{U}_c^{iv}}{\bar{U}_c'} + \left(\alpha^2 + \frac{\bar{U}_c'''}{\bar{U}_c'}\right)a_1\right]Y(A^{\dagger}\mathrm{e}^{\mathrm{i}\alpha\zeta} + \mathrm{c.c.})\right. \\ & - \sum_m\left(m^2\alpha^2 + \frac{\bar{U}_c'''}{\bar{U}_c'}\right)(b_2^{(m)}\mathrm{e}^{\mathrm{i}m\alpha\zeta} + \mathrm{c.c.}) \\ & \left. - \left[-2\mathrm{i}\alpha c^{-1}\frac{\partial A^{\dagger}}{\partial\bar{x}} + \frac{\mathrm{i}\bar{U}_c'''}{\alpha\bar{U}_c'^2}\chi_a\mathscr{D}_0A^{\dagger}\right]\mathrm{e}^{\mathrm{i}\alpha\zeta} + \mathrm{c.c.}\right\},\end{aligned} \tag{2.43}$$

equation (2.42) simplifies to

$$\begin{aligned}\mathscr{L}_{\mathscr{N}}\Omega_3^{\dagger} = {} & -\frac{\bar{U}_c'''}{\bar{U}_c'}\mathscr{D}_0\left[\sum b_2^{(m)}\mathrm{e}^{\mathrm{i}m\alpha\zeta} + \mathrm{c.c.}\right] - \frac{\mathrm{i}\bar{U}_c'''}{\alpha\bar{U}_c'^2}\chi_a\mathscr{D}_0^2A^{\dagger}\mathrm{e}^{\mathrm{i}\alpha\zeta} + \mathrm{c.c.} \\ & - c^{-1}\bar{U}_c'Y\frac{\partial\Omega^{\dagger}}{\partial\bar{x}} + \left[\sum_m \mathrm{i}m\alpha b_2^{(m)}\mathrm{e}^{m\mathrm{i}\alpha\zeta}\right. \\ & \left. + \left(\mathrm{i}\alpha a_1YA^{\dagger} + c^{-1}\frac{\partial A^{\dagger}}{\partial\bar{x}}\right)\mathrm{e}^{\mathrm{i}\alpha\zeta} + \mathrm{c.c.}\right]\frac{\partial\Omega^{\dagger}}{\partial Y} \\ & - (a_1A^{\dagger}\mathrm{e}^{\mathrm{i}\alpha\zeta} + \mathrm{c.c.})\frac{\partial\Omega^{\dagger}}{\partial\zeta} + \frac{1}{2}\frac{\bar{U}_c^{iv}}{\bar{U}_c'}(\mathrm{i}\alpha A^{\dagger 2}\mathrm{e}^{2\mathrm{i}\alpha\zeta} + \mathrm{c.c.}).\end{aligned} \tag{2.44}$$

Matching of the $O(\epsilon^2)$ streamwise velocity of the fundamental component leads to

$$\frac{\alpha}{2\pi}\int_{-\infty}^{\infty}\int_{0}^{2\pi/\alpha}\Omega_3^{\dagger}\mathrm{e}^{-\mathrm{i}\alpha\zeta}\,\mathrm{d}\zeta\,\mathrm{d}Y=\left\{-\mathrm{i}\alpha^{-1}J_2\frac{\partial B^{\dagger}}{\partial\tau}+\mathrm{i}(2\alpha c^{-1}J_1-\alpha^{-1}J_2)\frac{\partial B^{\dagger}}{\partial\bar{x}}\right\}$$
$$-\gamma_{11}\frac{\partial^2 A^{\dagger}}{\partial\bar{x}^2}-\gamma_{12}\frac{\partial^2 A^{\dagger}}{\partial\tau\partial\bar{x}}-\gamma_{22}\frac{\partial^2 A^{\dagger}}{\partial\tau^2}. \tag{2.45}$$

The system (2.44)–(2.45) determines the function $B^{\dagger}$, which is needed in order to obtain the streamwise velocity accurate up to $O(\epsilon^{1/2})$.

3. The coupled evolution systems

Equations (2.38) and (2.40) form the system that governs the nonlinear evolution of the disturbance. It is convenient to introduce the normalized variables

$$\bar{\eta}=\alpha\bar{U}_c'Y,\quad \bar{\zeta}=\alpha\zeta,\quad \bar{\lambda}=(\alpha\bar{U}_c')^2\lambda,\quad \Omega=\Omega^{\dagger}(\alpha\bar{U}_c')^2/\bar{U}_c''',\quad \bar{A}=\alpha^2\bar{U}_c'A^{\dagger}, \tag{3.1}$$

where we assume that $\bar{U}_c'>0$. Then (2.38) and (2.40) become

$$\left.\begin{aligned}&\left[\frac{\partial}{\partial\tau}+\frac{\partial}{\partial\bar{x}}+\bar{\eta}\frac{\partial}{\partial\bar{\zeta}}-(\mathrm{i}\bar{A}\mathrm{e}^{\mathrm{i}\bar{\zeta}}+\mathrm{c.c.})\frac{\partial}{\partial\bar{\eta}}-\bar{\lambda}\frac{\partial^2}{\partial\bar{\eta}^2}\right]\Omega=-(\mathscr{D}_0\bar{A}\mathrm{e}^{\mathrm{i}\bar{\zeta}}+\mathrm{c.c.}),\\&\frac{1}{2\pi}\int_{-\infty}^{\infty}\int_{0}^{2\pi}\Omega\mathrm{e}^{-\mathrm{i}\bar{\zeta}}\,\mathrm{d}\bar{\zeta}\,\mathrm{d}\bar{\eta}=\Lambda_1\frac{\partial\bar{A}}{\partial\tau}+\Lambda_2\frac{\partial\bar{A}}{\partial\bar{x}},\end{aligned}\right\} \tag{3.2}$$

where we have put

$$\Lambda_1=-\mathrm{i}J_2\bar{U}_c'^2/\bar{U}_c''',\quad \Lambda_2=\mathrm{i}(2\alpha^2c^{-1}J_1-J_2)\bar{U}_c'^2/\bar{U}_c'''. \tag{3.3}$$

The most significant feature of the present theory is the combined non-equilibrium and nonlinear effects: the transverse distribution of the disturbance (e.g. the critical-layer vorticity) is continually distorted and evolves nonlinearly over the same time and length scales as the amplitude does. Now if we write the complex amplitude A as $A=a\mathrm{e}^{\mathrm{i}p}$, the modulations of the real amplitude a and phase p are mutually coupled, and both play an active role in the nonlinear evolution. This is contrast to the classical weakly nonlinear theory and the energy method, which form the basis of some previous models for spectral dynamics. There the transverse shape of the disturbance is given by the eigenfunction and remains invariant during the evolution, and the phase modulation is dynamically passive in the sense that it is completely determined by the amplitude (Wu 2004).

3.1. *Upstream condition*

Let us now consider what condition could be imposed upstream as an 'initial condition'. As $\bar{x}\to-\infty$, the disturbance is small so that the nonlinear term in the first equation of (3.2) can be neglected. Solving the linearized equation, we find that

$$\Omega\sim\left\{-\int_0^{\infty}\mathscr{D}_0\bar{A}(\bar{x}-\xi,\tau-\xi)\mathrm{e}^{-(1/3)\bar{\lambda}\xi^3-\mathrm{i}\bar{\eta}\xi}\,\mathrm{d}\xi\right\}\mathrm{e}^{\mathrm{i}\bar{\zeta}}+\mathrm{c.c.}, \tag{3.4}$$

from which it follows that

$$\int_{-\infty}^{\infty}\Omega\,\mathrm{d}\bar{\eta}=-\pi\mathscr{D}_0\bar{A}. \tag{3.5}$$

This result is inserted into the second equation of (3.2) to give

$$\frac{\partial \bar{A}}{\partial \tau} + c_g \frac{\partial \bar{A}}{\partial \bar{x}} = 0, \tag{3.6}$$

where the group velocity

$$c_g = 1 - 2\alpha^2 c^{-1} J_1 \Big/ \left\{ \frac{\mathrm{i}\pi \bar{U}_c'''}{\bar{U}_c' |\bar{U}_c'|} + J_2 \right\}. \tag{3.7}$$

Note that since c_g is a complex number, it is impossible to introduce a coordinate moving with the group velocity. As such the modulation equation must be of first order rather than second order, as would have been the case if the group velocity were real.

A particular case where the disturbance has a discrete spectrum corresponds to the initial perturbation consisting of three waves of the sideband type. Then

$$\bar{A} \sim \left\{ a_0^+ \mathrm{e}^{\kappa^+ \bar{x} - \mathrm{i}\Delta\tau} + a_0 \mathrm{e}^{\kappa \bar{x}} + a_0^- \mathrm{e}^{\mathrm{i}\varphi_0} \mathrm{e}^{\kappa^- \bar{x} + \mathrm{i}\Delta\tau} \right\} \mathrm{e}^{-\mathrm{i}S_0\tau}, \tag{3.8}$$

where $\kappa = \mathrm{i}S_0/c_g$, and $\kappa^\pm = \mathrm{i}(S_0 \pm \Delta)/c_g$ with S_0 representing the scaled deviation of the central mode frequency from the neutral frequency $\alpha_0 c$; see (2.4). With the carrier-wave factor taken into account, the above initial condition represents three waves with frequencies $\omega_0 = (\alpha_0 c + \epsilon^{1/2} S_0)$ and $\omega^\pm = (\omega_0 \pm \epsilon^{1/2}\Delta)$; the frequency difference $\omega_v = \epsilon^{1/2}\Delta$. The constants a_0 and $a_0^\pm$ are the re-scaled initial amplitudes, while φ_0 characterizes the phase difference. If only two of these three waves are excited, as in the experiments of Sato (1970) and Miksad *et al.* (1982), we may set one of $a_0^\pm$ to zero or a small value. Substitution of (3.8) into (3.4) yields

$$\Omega \sim \left(a_0^+ \Pi_0^+ \mathrm{e}^{\kappa^+ \bar{x} - \mathrm{i}\Delta\tau} + a_0 \Pi_0 \mathrm{e}^{\kappa \bar{x}} + a_0^- \mathrm{e}^{\mathrm{i}\varphi_0} \Pi_0^- \mathrm{e}^{\kappa^- \bar{x} + \mathrm{i}\Delta\tau} \right) \mathrm{e}^{-\mathrm{i}S_0\tau + \mathrm{i}\bar{\zeta}} + \text{c.c.}, \tag{3.9}$$

where

$$\Pi_0^\pm = -\left[\kappa^\pm - \mathrm{i}(S_0 \pm \Delta)\right] \int_0^\infty \exp\left\{ -\frac{1}{3}\bar{\lambda}\xi^3 - \mathrm{i}[\bar{\eta} - (S_0 \pm \Delta) - \mathrm{i}\kappa^\pm]\xi \right\} \mathrm{d}\xi, \tag{3.10}$$

and Π_0 has the same expression as above provided that Δ is set to zero.

As $\bar{x} \to -\infty$, A and Ω are approximated respectively by (3.8) and (3.9), which represent the appropriate upstream condition pertaining to the experiments of Sato (1970) and Miksad *et al.* (1982). The objective of the present paper is to investigate how this form of disturbance evolves nonlinearly, with the particular interest in the generation of different spectral components and their role in flow randomization.

3.2. *Fourier decomposition of the solution and boundary condition*

It is convenient to write the the solution for $\bar{A}$ and Ω as

$$\bar{A} = A\mathrm{e}^{-\mathrm{i}S_0\tau}, \quad \Omega = \sum_{n=-\infty}^{\infty} Q_n(\tau, \bar{x}, \eta) \mathrm{e}^{\mathrm{i}n(\bar{\zeta} - S_0\tau)} \quad \text{with } Q_{-n} = Q_n^*, \tag{3.11}$$

where $\eta = \bar{\eta} - S_0$. Then Q_n $(n = 0, 1, 2, \ldots)$ satisfy the coupled system of equations,

$$\left(\frac{\partial}{\partial \tau} + \frac{\partial}{\partial \bar{x}} + \mathrm{i}n\eta - \bar{\lambda} \frac{\partial^2}{\partial \eta^2} \right) Q_n + \mathrm{i} \frac{\partial}{\partial \eta} (A^* Q_{n+1} - A Q_{n-1}) = -\delta_{n1} (\mathscr{D}_0 - \mathrm{i}S_0) A, \tag{3.12}$$

$$\int_{-\infty}^{\infty} Q_1 \, \mathrm{d}\eta = -\mathrm{i}S_0 \Lambda_1 A + \Lambda_1 \frac{\partial A}{\partial \tau} + \Lambda_2 \frac{\partial A}{\partial \bar{x}}. \tag{3.13}$$

It follows from (3.12) that as $\eta \to \pm\infty$,

$$Q_1 \to \left\{ \frac{\mathrm{i}}{\eta} - \frac{\mathscr{D}_0}{\eta^2} - \frac{\mathrm{i}\mathscr{D}_0^2}{\eta^3} \right\} (\mathscr{D}_0 - \mathrm{i}S_0)A + O(\eta^{-4}), \tag{3.14}$$

$$Q_0 \to -\frac{|A|^2}{\eta^2} + \frac{2\mathrm{i}}{\eta^3} \left\{ A\mathscr{D}_0 A^* - A^*\mathscr{D}_0 A + \mathrm{i}S_0 |A|^2 \right\} + O(\eta^{-4}), \tag{3.15}$$

$$Q_2 \to -\frac{\mathrm{i}}{2\eta^3} A(\mathscr{D}_0 - \mathrm{i}S_0)A + O(\eta^{-4}). \tag{3.16}$$

Due to the slow decay of Q_1, the integral in (3.13) must be interpreted as a Cauchy principal value. The infinite domain in the η-direction is truncated to a large but finite interval $-H \leqslant \eta \leqslant H$. Then (3.13) can be written as

$$-\mathrm{i}S_0\Lambda_1 A + \Lambda_1 \frac{\partial A}{\partial \tau} + \Lambda_2 \frac{\partial A}{\partial \bar{x}} = I_{10} - \frac{2}{H}\mathscr{D}_0(\mathscr{D}_0 - \mathrm{i}S_0)A + O(H^{-3}), \tag{3.17}$$

where we have defined

$$I_{nk} = \int_{-H}^{H} \eta^k Q_n \, \mathrm{d}\eta. \tag{3.18}$$

The second-order derivative with respect to $\bar{x}$ in (3.17) is inconvenient for numerical integration. Using a similar procedure to that in Goldstein & Hultgren (1988), we obtain a first-order system with respect to $\bar{x}$ (see appendix A for the derivation):

$$\begin{aligned} &\tilde{\Lambda}_1 \frac{\partial A}{\partial \tau} + \tilde{\Lambda}_2 \frac{\partial A}{\partial \bar{x}} - \left(\tilde{\Lambda}_{d,1} \frac{\partial^2}{\partial \tau^2} + \tilde{\Lambda}_{d,2} \frac{\partial^2}{\partial \tau \partial \bar{x}} \right) A + \tilde{\Lambda}_0 A \\ &\quad = \left(q - \frac{2\Lambda_d}{H\Lambda_2} \frac{\partial}{\partial \tau} \right) I_{10} + \frac{2\mathrm{i}}{H} I_{11} - \frac{4}{H^2\Lambda_2}(I_{12} - A^* I_{20}), \end{aligned} \tag{3.19}$$

where

$$\tilde{\Lambda}_1 = \left(\Lambda_1 - \frac{2\mathrm{i}S_0}{H} \right) q - 2\left[2 - \frac{\mathrm{i}S_0\Lambda_1}{H} + \frac{4\mathrm{i}S_0}{\Lambda_2 H} \right] + \frac{2\mathrm{i}S_0\Lambda_1\Lambda_d}{H\Lambda_2}, \tag{3.20}$$

$$\tilde{\Lambda}_2 = \left(\Lambda_2 - \frac{2\mathrm{i}S_0}{H} \right) q - 2\left[2 - \frac{\mathrm{i}S_0\Lambda_1}{H} + \frac{4\mathrm{i}S_0}{\Lambda_2 H} \right], \tag{3.21}$$

$$\tilde{\Lambda}_{d,j} = \frac{2\Lambda_d}{H}\left[1 - \frac{2\mathrm{i}S_0}{H\Lambda_2} + \frac{\Lambda_j}{\Lambda_2} \right] \quad (j = 1, 2), \qquad \tilde{\Lambda}_0 = -\mathrm{i}S_0\Lambda_1 q + 4\mathrm{i}S_0, \tag{3.22}$$

$$q = \Lambda_2 - \frac{2\mathrm{i}S_0}{H} - \frac{4}{\Lambda_2} + \frac{2\mathrm{i}S_0\Lambda_1}{H\Lambda_2}. \tag{3.23}$$

For the initial perturbation of the sideband form (3.8), A and Q_n take the form

$$A = \sum_{m=-\infty}^{\infty} A_m(\bar{x})\mathrm{e}^{-\mathrm{i}m\Delta\tau}, \quad Q_n = \sum_{m=-\infty}^{\infty} Q_n^{(m)}(\bar{x}, \eta)\mathrm{e}^{-\mathrm{i}m\Delta\tau}. \tag{3.24}$$

Substitution of (3.24) into (3.12) and (3.19) gives the equations for $Q_n^{(m)}$ and A_m,

$$\left.\begin{aligned}
&\left[-\mathrm{i}m\Delta + \frac{\partial}{\partial\bar{x}} + \mathrm{i}n\eta - \bar{\lambda}\frac{\partial^2}{\partial\eta^2}\right] Q_n^{(m)} - \mathrm{i}\sum_{k=-\infty}^{\infty}(A_k Q_{n-1,\eta}^{(m-k)} - A_k^* Q_{n+1,\eta}^{(m+k)}) \\
&\quad = -\delta_{n1}\left[\frac{\partial}{\partial\bar{x}} - \mathrm{i}(S_0 + m\Delta)\right] A_m, \\
&(\tilde{\Lambda}_2 + \mathrm{i}m\tilde{\Lambda}_{d,2}\Delta)\frac{\partial A_m}{\partial\bar{x}} + (\tilde{\Lambda}_0 - \mathrm{i}m\tilde{\Lambda}_1\Delta + m^2\tilde{\Lambda}_{d,1}\Delta^2)A_m \\
&\quad = \left[q + \frac{2\Lambda_d}{H\Lambda_2}(\mathrm{i}m\Delta)\right] I_{10}^{(m)} + \frac{2\mathrm{i}}{H} I_{11}^{(m)} - \frac{4}{H^2\Lambda_2}\left\{I_{12}^{(m)} - \sum_{k=-\infty}^{\infty} A_k^* I_{20}^{(m+k)}\right\},
\end{aligned}\right\} \tag{3.25}$$

where $I_{10}^{(m)}$, $I_{11}^{(m)}$, $I_{12}^{(m)}$ and $I_{20}^{(m)}$ denote the Fourier series coefficients of I_{nk} defined by (3.18). It follows from $Q_{-n} = Q_n^*$ that $Q_{-n}^{(m)} = Q_n^{(-m)*}$, and so it is only necessary to solve the system for $n \geqslant 0$.

The evolution system (2.44)–(2.45) for $B^\dagger$ and $\Omega_3^\dagger$ can be re-scaled accordingly. The solution form as well as the boundary and initial conditions are discussed in appendix B.

4. Linear sideband instability

Amplification of sideband components due to their mutual interactions is a rather generic instability that may occur in a great variety of wave systems. As was demonstrated by Stuart & Diprima (1978), it can be studied most conveniently by using the appropriate nonlinear evolution equations for the modulated wavetrain or wavepacket (e.g. nonlinear Schrödinger equation for water waves). The monochromatic wave serves as the base state, and is perturbed by disturbances in its spectral sideband. The equations for the disturbances follow from linearizing the modulation equation about the base state. Sideband interaction/instability has been suggested as a possible mechanism responsible for the observed spectral broadening in transitional free shear layers. We now study this instability mathematically using the evolution system presented in the previous section.

The monochromatic wave corresponds to a single-frequency disturbance, for which $\bar{A} = A_0(\bar{x})\mathrm{e}^{-\mathrm{i}S_0\tau}$. The amplitude $A_0(\bar{x})$ and the associated vorticity Ω_0 are then governed by the limiting form of (3.2) in which $\partial/\partial\tau$ is replaced by $(-\mathrm{i}S_0)$. This is the case studied by Goldstein & Leib (1988) and Goldstein & Hultgren (1988), who solved the resultant system by expressing Ω_0 as a Fourier series,

$$\Omega_0 = \sum_{n=-\infty}^{\infty} Q_n^{(0)}(\bar{x}, \eta)\mathrm{e}^{\mathrm{i}n\tilde{\zeta}} \quad \text{with } \tilde{\zeta} = \bar{\zeta} - S_0\tau. \tag{4.1}$$

Their results show that the disturbance rolls up to form concentrated vortices, or spanwise 'rollers'. Now we study the linear stability of these vortices by writing

$$\bar{A} = A_0(\bar{x})\mathrm{e}^{-\mathrm{i}S_0\tau} + \delta\tilde{A}(\tau, \bar{x})\mathrm{e}^{-\mathrm{i}S_0\tau}, \quad \Omega = \Omega_0 + \delta\tilde{\Omega} \quad \text{with } \delta \ll O(1). \tag{4.2}$$

Then we obtain the linearized system

$$\left.\begin{aligned}&\left[\frac{\partial}{\partial\tau}+\frac{\partial}{\partial\bar{x}}+\eta\frac{\partial}{\partial\tilde{\zeta}}-(\mathrm{i}A_0\mathrm{e}^{\mathrm{i}\tilde{\zeta}}+\mathrm{c.c.})\frac{\partial}{\partial\eta}-\bar{\lambda}\frac{\partial^2}{\partial\eta^2}\right]\tilde{\Omega}-\Omega_{0,\eta}(\mathrm{i}\tilde{A}\mathrm{e}^{\mathrm{i}\tilde{\zeta}}+\mathrm{c.c.})\\&\quad=-\left(\frac{\partial}{\partial\tau}+\frac{\partial}{\partial\bar{x}}-\mathrm{i}S_0\right)\tilde{A}\mathrm{e}^{\mathrm{i}\tilde{\zeta}}+\mathrm{c.c.},\\&\frac{1}{2\pi}\int_{-\infty}^{\infty}\int_0^{2\pi}\tilde{\Omega}\mathrm{e}^{-\mathrm{i}\tilde{\zeta}}\,\mathrm{d}\tilde{\zeta}\,\mathrm{d}\eta=-\mathrm{i}S_0\Lambda_1\tilde{A}+\Lambda_1\frac{\partial\tilde{A}}{\partial\tau}+\Lambda_2\frac{\partial\tilde{A}}{\partial\bar{x}}.\end{aligned}\right\}\tag{4.3}$$

For a disturbance of the sideband type (3.8), we may write (see Stuart & Diprima 1978)

$$\tilde{A}=\tilde{A}^{+}\mathrm{e}^{-\mathrm{i}\Delta\tau}+\tilde{A}^{-}\mathrm{e}^{\mathrm{i}\Delta\tau},\quad\tilde{\Omega}=\tilde{\Omega}^{+}(\tilde{\zeta},\bar{x},\eta)\mathrm{e}^{-\mathrm{i}\Delta\tau}+\tilde{\Omega}^{-}(\tilde{\zeta},\bar{x},\eta)\mathrm{e}^{\mathrm{i}\Delta\tau}.\tag{4.4}$$

Substitution of (4.4) into (4.3) yields the equations governing $\tilde{A}^{\pm}$ and $\tilde{\Omega}^{\pm}$,

$$\left.\begin{aligned}&\left[\frac{\partial}{\partial\bar{x}}+\eta\frac{\partial}{\partial\tilde{\zeta}}\mp\mathrm{i}\Delta-(\mathrm{i}A_0\mathrm{e}^{\mathrm{i}\tilde{\zeta}}+\mathrm{c.c.})\frac{\partial}{\partial\eta}-\bar{\lambda}\frac{\partial^2}{\partial\eta^2}\right]\tilde{\Omega}^{\pm}-\mathrm{i}(\tilde{A}^{\pm}\mathrm{e}^{\mathrm{i}\tilde{\zeta}}-\tilde{A}^{\mp*}\mathrm{e}^{-\mathrm{i}\tilde{\zeta}})\Omega_{0,\eta}\\&\quad=-\left[\frac{\partial}{\partial\bar{x}}-\mathrm{i}(S_0\pm\Delta)\right]\tilde{A}^{\pm}\mathrm{e}^{\mathrm{i}\tilde{\zeta}}-\left[\frac{\partial}{\partial\bar{x}}+\mathrm{i}(S_0\mp\Delta)\right]\tilde{A}^{\mp*}\mathrm{e}^{-\mathrm{i}\tilde{\zeta}},\\&\frac{1}{2\pi}\int_{-\infty}^{\infty}\int_0^{2\pi}\tilde{\Omega}^{\pm}\mathrm{e}^{-\mathrm{i}\tilde{\zeta}}\,\mathrm{d}\tilde{\zeta}\,\mathrm{d}\eta=-\mathrm{i}(S_0\pm\Delta)\Lambda_1\tilde{A}^{\pm}+\Lambda_2\frac{\partial\tilde{A}^{\pm}}{\partial\bar{x}}.\end{aligned}\right\}\tag{4.5}$$

It is of interest to compare the present sideband instability with the more familiar one for an equilibrium wave. Firstly, since the basic state, the roller structure, evolves on the same length scale as the perturbation, the instability must be formulated as an initial-value rather than an eigenvalue problem. Secondly, due to the strongly nonlinear nature of vorticity rollers, the evolution of the sideband perturbation is governed by a parametrically excited system as opposed to a system with constant coefficients. Note that the central mode acts, through $A_0\mathrm{e}^{\mathrm{i}\tilde{\zeta}}$ and $\Omega_{0,\eta}$, as the 'parametric excitation' in the system, while the difference mode, represented by $Q_0^{\pm}$, is continually generated by the interaction and evolves as part of the sideband perturbation. The present theory is therefore conceptually different from the model of Hajj (1997), where the difference mode was specified as part of the base state and contributes the parametric excitation.

The equations for $\tilde{\Omega}^{\pm}$ are the complex conjugate to each other, consistent with $\tilde{\Omega}^{-}=\tilde{\Omega}^{+*}$ for reality of $\tilde{\Omega}$. The function $\tilde{\Omega}^{\pm}$ may further be decomposed into a Fourier series

$$\tilde{\Omega}^{\pm}=\sum_{n=-\infty}^{\infty}Q_n^{\pm}\mathrm{e}^{\mathrm{i}n\tilde{\zeta}},\tag{4.6}$$

with the coefficients obeying the relation, $Q_{-n}^{+}=Q_n^{-*}$, in order for $\tilde{\Omega}^{\pm}$ to be real. Inserting into the vorticity equation in (4.5), we obtain

$$\begin{aligned}&\left[\mp\mathrm{i}\Delta+\frac{\partial}{\partial\bar{x}}+\mathrm{i}n\eta-\bar{\lambda}\frac{\partial^2}{\partial\eta^2}\right]Q_n^{\pm}-(\mathrm{i}A_0Q_{n-1,\eta}^{\pm}-\mathrm{i}A_0^{*}Q_{n+1,\eta}^{\pm})\\&\quad=(\mathrm{i}\tilde{A}^{\pm}Q_{n-1,\eta}^{(0)}-\mathrm{i}\tilde{A}^{\mp*}Q_{n+1,\eta}^{(0)})-\delta_{n1}\left[\frac{\partial}{\partial\bar{x}}-\mathrm{i}(S_0\pm\Delta)\right]\tilde{A}^{\pm}\quad(n=0,1,2,\ldots).\end{aligned}\tag{4.7}$$

It follows from (3.19) that the equations for $\tilde{A}^{\pm}$ may be approximated as

$$(\tilde{\Lambda}_2 \pm \mathrm{i}\tilde{\Lambda}_{d,2}\Delta)\frac{\partial \tilde{A}^{\pm}}{\partial \bar{x}} + (\tilde{\Lambda}_0 \mp \mathrm{i}\tilde{\Lambda}_1\Delta + \tilde{\Lambda}_{d,1}\Delta^2)\tilde{A}^{\pm}$$
$$= [q \pm \mathrm{i}\Delta\Lambda_d/(H\Lambda_2)]\, I_{10}^{\pm} + \frac{2\mathrm{i}}{H} I_{11}^{\pm} - \frac{4}{H^2\Lambda_2}\left\{ I_{12}^{\pm} - (\tilde{A}^{\mp *} I_{20}^{(0)} + A_0^* I_{20}^{\pm}) \right\}. \quad (4.8)$$

The boundary condition for $Q_n^{\pm}$ is derived by inserting (4.2) and (4.4) with (4.6) into (3.14)–(3.16). We find that for $\eta \gg O(1)$,

$$Q_1^{\pm} \sim \frac{\mathrm{i}}{\eta}\left(\frac{\partial}{\partial \bar{x}} \mp \mathrm{i}\Delta - \mathrm{i}S_0\right)\tilde{A}^{\pm} - \frac{1}{\eta^2}\left(\frac{\partial}{\partial \bar{x}} \mp \mathrm{i}\Delta\right)\left(\frac{\partial}{\partial \bar{x}} \mp \mathrm{i}\Delta - \mathrm{i}S_0\right)\tilde{A}^{\pm}, \quad (4.9a)$$

$$Q_0^{\pm} \sim -\frac{1}{\eta^2}(A_0^*\tilde{A}^{\pm} + A_0\tilde{A}^{\mp *})$$
$$+ \frac{2\mathrm{i}}{\eta^3}\left\{ \tilde{A}^{\pm}\frac{\partial A_0^*}{\partial \bar{x}} + A_0\left(\frac{\partial}{\partial \bar{x}} \mp \mathrm{i}\Delta\right)\tilde{A}^{\mp *} - \text{c.c.} + \mathrm{i}S_0(A_0^*\tilde{A}^{\pm} + A_0\tilde{A}^{\mp *}) \right\}, \quad (4.9b)$$

$$Q_2^{\pm} \sim -\frac{\mathrm{i}}{2\eta^3}\left\{ \tilde{A}^{\pm}\frac{\partial A_0}{\partial \bar{x}} + A_0\left(\frac{\partial}{\partial \bar{x}} \mp \mathrm{i}\Delta\right)\tilde{A}^{\pm} - 2\mathrm{i}S_0 A_0\tilde{A}^{\pm} \right\}. \quad (4.9c)$$

The nonlinear evolution system governing the base state, (Ω_0, A_0), could be solved beforehand, but it is more convenient to solve it simultaneously with the linearized system (4.7)–(4.8) for the sideband perturbations.

5. Numerical results

The numerical work consists of solving (3.25) and (4.7)–(4.8). A predictor–corrector method was employed, and is now explained with reference to the former system since the latter may be treated as a special case. The amplitude equations for A_m are discretized using the fourth-order explicit (Adams–Bashforth) and implicit (Adams–Moulton) schemes to construct the predictor and corrector respectively. The integrals are evaluated using Simpson's rule. The vorticity equations for $Q_n^{(m)}$ are discretized by the Crank–Nicolson scheme. The boundary conditions are imposed according to the far-field behaviour (3.14)–(3.16). A new feature for a modulated wavetrain is that the equations and boundary conditions involve products of the series with respect to $\mathrm{e}^{-\mathrm{i}m\Delta\tau}$, and these were evaluated by using the fast Fourier transform algorithm. The system (3.25) is truncated with $0 \leqslant n \leqslant N$ and $-M \leqslant m \leqslant M$, and solved in a large but finite domain $-H \leqslant \eta \leqslant H$. The calculations were mostly performed for $M = 20$, $N = 8$, $H = 60$, the 'time' step $\Delta\bar{x} = 2 \times 10^{-3}$ and the spatial mesh size $\Delta\eta = 0.1$. For the mixing layer and planar wake under consideration, the resolution proves adequate for $\bar{x}$ up to $\sim$15; within this range, increasing M, N and H respectively to 25, 16 and 80, or halving the 'time' step/mesh size, does not cause appreciable change to the results. The accuracy, however, deteriorates when $\bar{x} > 15$.

Before presenting numerical results, we list several relevant flow quantities. In addition to the amplitude function A, another quantity of interest is $\Omega_c^{\dagger}$, defined as (see Goldstein & Leib 1988)

$$\Omega_c^{\dagger} = \tfrac{1}{2}\bar{U}_c'''Y^2 + (\Psi_{2,YY} + \Psi_{0,\zeta\zeta}) = \tfrac{1}{2}\bar{U}_c'''Y^2 + \Omega^{\dagger} + (\bar{U}_c'''/\bar{U}_c')A^{\dagger}\mathrm{e}^{\mathrm{i}\bar{\zeta}} + \text{c.c.} \quad (5.1)$$

It will be referred to as the 'critical-layer vorticity' since $\bar{U}_c' + \epsilon\Omega_c^{\dagger}$ represents the total vorticity within the critical layer. For convenience, we will present the renormalized critical-layer vorticity,

$$\Omega_c \equiv \Omega_c^{\dagger}\,(\alpha\bar{U}_c')^2\,/\bar{U}_c''' = \tfrac{1}{2}\,(\eta + S_0)^2 + A\mathrm{e}^{\mathrm{i}\tilde{\zeta}} + \text{c.c.} + \Omega, \tag{5.2}$$

where use has been made of (3.1).

The streamwise velocity profiles of the harmonics within the critical layer

$$\widehat{u}_n \equiv \epsilon^{3/2}\left[a_2^{(n)} + \bar{U}_c'''/\,(\alpha\bar{U}_c')^3 \int_{-\infty}^{\eta} Q_n\,\mathrm{d}\eta\right] \quad (n = 2, 3, \ldots), \tag{5.3}$$

and the mean-flow distortion

$$\widehat{u}_0 \equiv \epsilon^{3/2}\int_{-\infty}^{Y} Q_0^{\dagger}\,\mathrm{d}Y = \epsilon^{3/2}\bar{U}_c'''/\,(\alpha\bar{U}_c')^3 \int_{-\infty}^{\eta} Q_0\,\mathrm{d}\eta. \tag{5.4}$$

The streamwise velocity of the fundamental component is given by

$$\begin{aligned}\widehat{u}_1 = {}& \epsilon a_1/(\alpha^2\bar{U}_c')A + \epsilon^{3/2}\left\{(\alpha^2 + \bar{U}_c'''/\bar{U}_c')\,(\alpha\bar{U}_c')^{-3}(\eta + S_0)A + a_2^{(1)-}\right\} \\ & + \epsilon^{3/2}\bar{U}_c'''/\,(\alpha\bar{U}_c')^3\left\{q_1 \ln\left[\epsilon^{1/2}/(\alpha\bar{U}_c')\right] + \lim_{H\to\infty}\left[q_1 \ln|H| + \int_{-H}^{\eta} Q_1\,\mathrm{d}\eta\right]\right\},\end{aligned} \tag{5.5}$$

where $q_1 = \mathrm{i}(\mathscr{D}_0 - \mathrm{i}S_0)A$. For each n, $\widehat{u}_n$ has a Fourier representation, $\widehat{u}_n = \sum_m \widehat{u}_n^{(m)}\mathrm{e}^{-\mathrm{i}m\Delta\tau}$. The instantaneous velocity in the critical layer is given by

$$\tilde{u}_c(\eta) = \sum_n \widehat{u}_n\mathrm{e}^{\mathrm{i}n\tilde{\zeta}} = \sum_{m,n}\widehat{u}_n^{(m)}\exp\{\mathrm{i}(n\zeta - (nS_0 + m\Delta)\tau)\}. \tag{5.6}$$

5.1. *Mixing layer*

The calculations are to be performed for the profile

$$\bar{U} = \bar{U}_c + \tanh y \quad \text{with } \bar{U}_c = (U_1 + U_2)/(U_1 - U_2), \tag{5.7}$$

where U_1 and U_2 represent the velocities of the two oncoming streams. For this profile,

$$\bar{U}_c' = 1, \quad \bar{U}_c''' = -2, \quad \phi_1 = \operatorname{sech} y, \quad \alpha = 1, \quad c = \bar{U}_c, \quad J_1 = 2, \quad J_2 = 0. \tag{5.8}$$

The equation (2.26) can be solved to obtain the solution for the harmonics $\phi_2^{(m)}$ in the main layer (Goldstein & Leib 1988),

$$\phi_2^{(m)} = J^{(m)}(\bar{x}, \tau)\mathrm{e}^{-m|y|}\left(1 + \frac{1}{m}\tanh|y|\right) \quad (m = 2, 3, \ldots), \tag{5.9}$$

where by matching $J^{(m)}$ is found as

$$J^{(m)} = \frac{mU_c'''}{2(1 - m^2)\,(\alpha U_c')^3}\int_{-\infty}^{\infty} Q_m\,\mathrm{d}\eta. \tag{5.10}$$

Using (2.21), we can find the solution for $\phi_2^{(1)}$, which is equivalent to (3.19) of Goldstein & Leib (1988).

We choose parameters pertaining to the experiments of Miksad (1972, 1973), where $U_1^* = 201$ cm s^{-1} and $U_2^* = 38$ cm s^{-1}. The amplitude $\epsilon = 0.2$ and Haberman

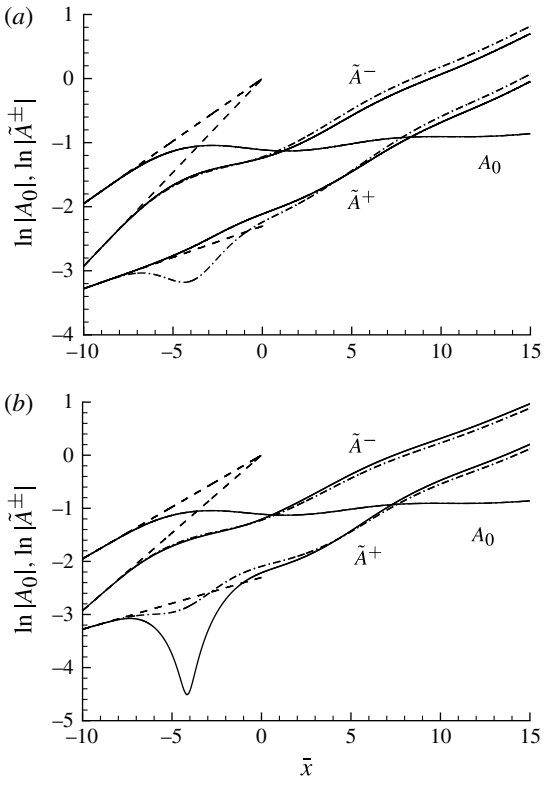

FIGURE 1. Development of the central mode $|A_0|$ and the sideband perturbations $|\tilde{A}^{\pm}|$ for $a_0^+/a_0^- = 0.1$ and different phase lag φ_0. (*a*) Solid lines, $\varphi_0 = \pi$; dash-dotted lines, $\varphi_0 = \pi/2$. (*b*) Solid lines, $\varphi_0 = 0$; dash-dotted lines, $\varphi_0 = -\pi/2$. The dashed lines represent the exponential growth of each component.

parameter $\bar{\lambda} = 0.0154$ were estimated from the fact that the maximum magnitude of the perturbation at $x^* = 5$ cm is approximately 0.06, as can be deduced from figure 18 of Miksad (1972). The frequency of the base wave is taken to be $\omega_0 = 5(\alpha c)/6$, i.e. $\epsilon^{1/2} S_0 = \alpha c/6$. The difference frequency $\omega_\nu = \epsilon^{1/2}\Delta = \alpha c/12$, giving a relative frequency difference of 10 %. This is considerably smaller than the experimental value of 25 %, but is chosen in order to apply the theory within its expected validity range. To study the sideband instability, we take $a_0^- = 1.0$ but first set $a_0^+ = 0.1$, a much smaller value in order to mimic two-frequency excitation experiments. The phase difference φ_0 is taken to be π, $\pi/2$, 0 and $-\pi/2$. In the following, the wave with the frequency ω_0 will be referred to as the 'central mode', while waves with frequencies $\omega^{\pm}$, or more generally with $\omega_0 \pm m\epsilon^{1/2}\Delta$, will be referred to as lower-band (minus sign) and upper-band (plus sign) components respectively. For brevity, we shall also refer to different components simply by their frequencies.

The first set of results to be presented (in figures 1–6) is concerned with the linear sideband instability. Figure 1 shows the development of the central mode amplitude A_0 and the sideband components $\tilde{A}_{\pm}$. Following an initial exponential growth in the linear stage, the base wave ω_0 saturates in a mildly oscillatory manner, as was found previously (Goldstein & Hultgren 1988). Meanwhile the sideband components start

to interact with each other through the central mode. As a result, the upper-band component ω^+, which has a smaller amplitude, is enhanced, while the initially stronger lower-band component ω^- is suppressed. We would like to point out that effects of 'enhancement'/'suppression' are distinguished according to whether the mode acquires at sufficiently large distances downstream an amplitude greater/smaller than could be reached via its linear growth. Consistent with experimental observations, the development of the sideband components is found to depend on the phase difference φ_0. Transient decay may occur for certain values of φ_0. For example, when $\varphi_0 = 0$, $\tilde{A}^+$ drops abruptly (figure 1*b*). However, in all cases the transient decay is more than compensated by the subsequent rapid growth. At large distances, the two sideband modes are 'synchronized', amplifying at the same rate, which is greater than κ^+ but less than κ^-. However, despite being promoted by the the interaction $\tilde{A}^+$ does not catch up with $\tilde{A}^-$, which remains the dominant mode.

As the central mode ω_0 evolves in a strongly nonlinear manner, the harmonics $m\omega_0$ appear simultaneously at the same order in its vorticity field Ω_0. Since the latter acts as the base state, the sideband perturbation consists of Fourier components with frequencies $m\omega_0 \pm \omega_\nu$, where m is an integer. Figure 2 shows contours of $\Omega_{0,c}$, the critical-layer vorticity of the central mode, at two typical locations $\bar{x} = -2$ and 5. The vorticity field features a fairly regular pattern that is characteristic of a viscous dominant critical layer. Also shown in the figure are streamwise velocity profiles of the sideband components $m\omega_0 \pm \omega_\nu$ $(m = 0, 2, 3)$, which are defined as

$$\left.\begin{aligned} u_m^{\pm} &= \left[a_2^{(n)} + \bar{U}_c'''/\left(\alpha \bar{U}_c'\right)^3 \int_{-\infty}^{\eta} Q_m^{\pm}\,\mathrm{d}\eta\right] \quad (m = 2, 3), \\ u_0 &= \bar{U}_c'''/\left(\alpha \bar{U}_c'\right)^3 \int_{-\infty}^{\eta} Q_0^{+}\,\mathrm{d}\eta. \end{aligned}\right\} \tag{5.11}$$

Clearly, the low-frequency component ω_ν and the lower-band component $2\omega_0 - \omega_\nu$ of the first harmonic acquire much larger amplitudes than others. At $\bar{x} = 5$, the magnitude of $2\omega_0 - \omega_\nu$ is about three times that of $2\omega_0 + \omega_\nu$.

The initial amplitude ratio a_0^+/a_0^- has a significant effect on the evolution of the sideband perturbations, as shown in figure 3. As a_0^+/a_0^- is increased, ω^+ is less enhanced. For $a_0^+/a_0^- = O(1)$, ω^+ is actually suppressed for a considerable distance, over which its amplitude is smaller than would be gained through its linear growth (figure 3*a*). The ω^- mode is also inhibited, but over a less extended distance (figure 3*b*). When a_0^+/a_0^- is appreciably larger than unity (e.g. $a_0^+/a_0^- = 3$), mode ω^+ remains suppressed, while mode ω^- might briefly amplify faster than its linear growth. In all cases, $\tilde{A}^-$ overtakes $\tilde{A}^+$, although this is shown in figure 3(*c*) only for $a_0^+/a_0^- = 0.6$ and 3.

In experiments often only two modes are excited, and this corresponds to either $a^+ = 0$ or $a^- = 0$. The development of the sideband perturbations in these two special cases is shown in figure 4. The comparison with the corresponding results for $a^+/a^- = 0.1$ and $a^-/a^+ = 0.1$ indicates that these are regular limiting cases, approached as $a^+/a^- \to 0$ and $a^-/a^+ \to 0$ respectively. When $a^+ = 0$ $(a^- = 0)$, the third component $\tilde{A}^+$ $(\tilde{A}^-)$ is generated by the nonlinear interaction, reaffirming the triadic nature of the sideband interaction. Once $\tilde{A}^+$ $(\tilde{A}^-)$ acquires a large enough magnitude, the evolution becomes quite similar to that in three-mode excitation.

Several important and general features of the sideband interaction may be noted. The evolution of sideband perturbations is highly non-equilibrium in the sense that their instantaneous amplification varies considerably and exhibits rather complex

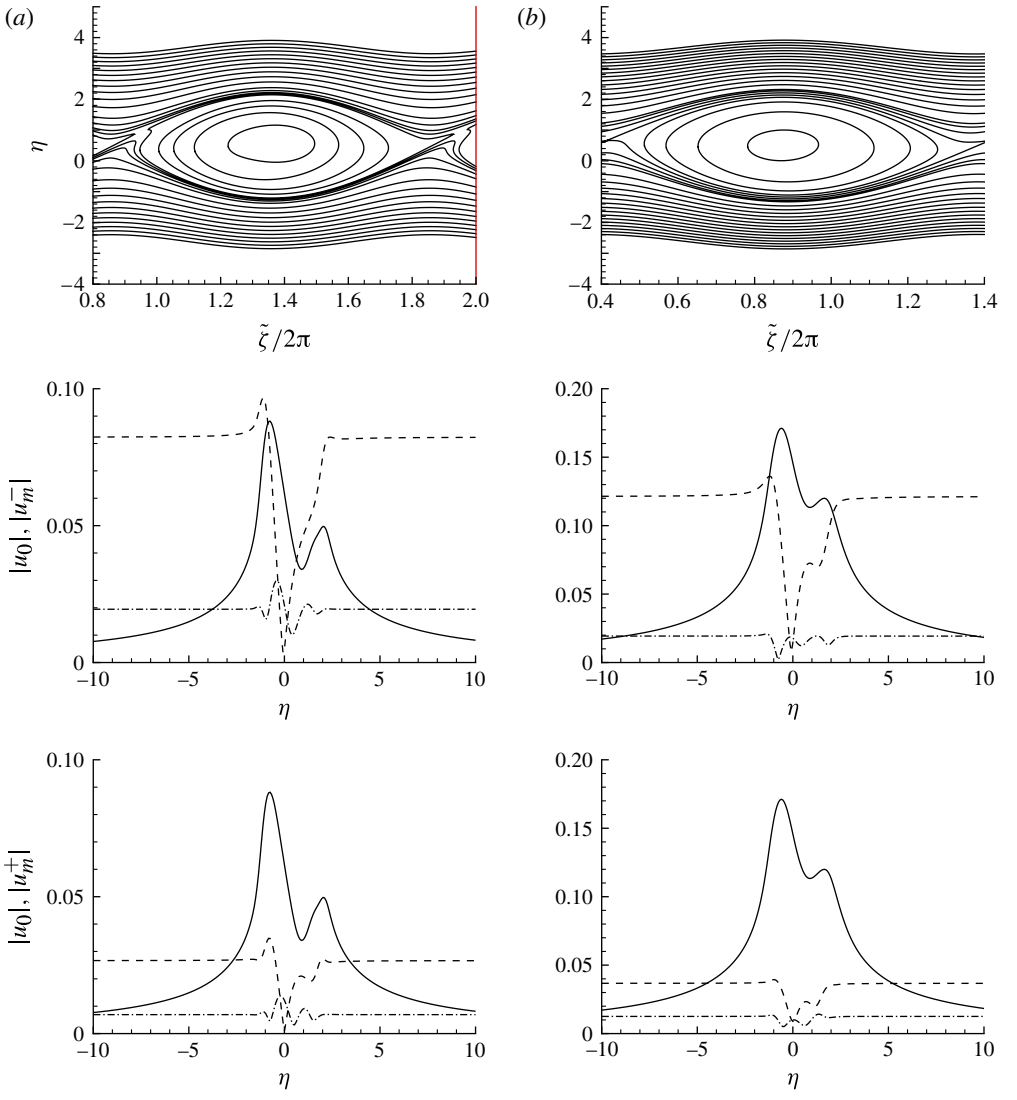

FIGURE 2. Contours of critical-layer vorticity $\Omega_{0,c}$ of the central mode and the streamwise velocity profiles $u_m^{\pm}$ (see (5.11)) of sideband components $(m\omega_0 \pm \omega_v)$ at (a) $x = -2$ and (b) 5. Solid lines, difference-frequency component $|u_0|$; dashed lines, $|u_2^{\pm}|$; dash-dotted lines, $|u_3^{\pm}|$.

behaviours. The sideband interaction tends to suppress the sideband mode with a larger amplitude while moderately enhancing the other mode, unlike the conventional sideband interaction where both sideband modes are destabilized and amplify at a constant rate. Since the suppression is exerted by the central mode, which always has the largest amplitude, the present result must be interpreted as the component with a larger amplitude (i.e. the central mode) inhibiting the component with a smaller amplitude (i.e. stronger one of the two sideband modes), consistent with the experimental finding. For any a_0^+/a_0^-, it is the lower-band component ω^- that is dominant over the upper-band component ω^+; this is so even when the latter

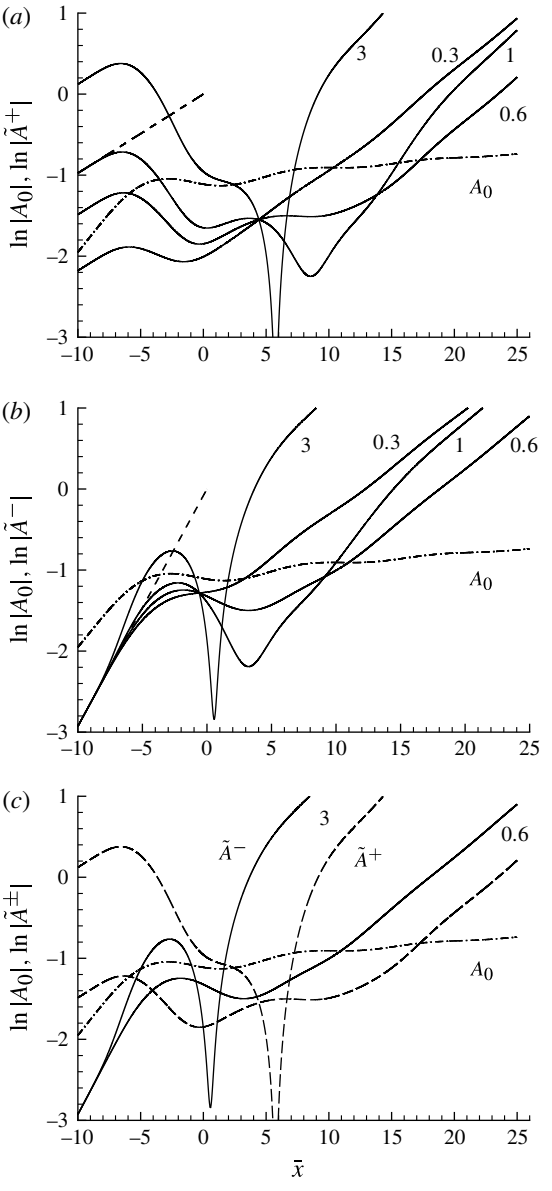

FIGURE 3. Development of the sideband perturbation for different initial amplitude ratios $a_0^+/a_0^- = 0.3,\ 0.6,\ 1$ and 3. The phase difference $\varphi_0 = \pi$. The dashed lines in (*a*) and (*b*) represent the exponential growth of each sideband component.

initially has a larger magnitude. The self-interaction of the central mode leads to attenuation of itself, but its interaction with the sideband modes causes the latter to amplify eventually at a synchronized rate. It is primarily in this sense that the present sideband instability exists. The non-equilibrium effect is instrumental for the sideband interaction to exhibit the suppression effect on one hand, and to act as an instability mechanism on the other.

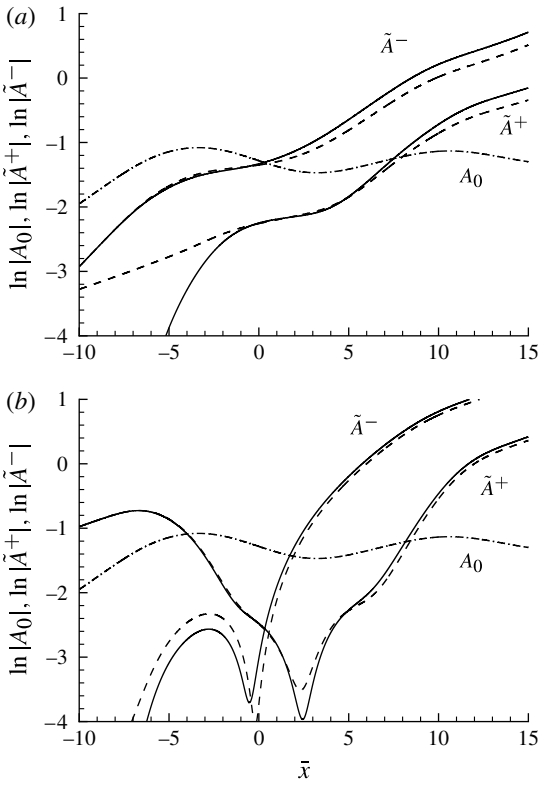

FIGURE 4. Development of the sideband perturbation in the cases of two-mode excitation: (*a*) $a^+ = 0$ and (*b*) $a^- = 0$. The dashed lines represent the results for $a^+/a^- = 0.1$ and $a^-/a^+ = 0.1$ respectively.

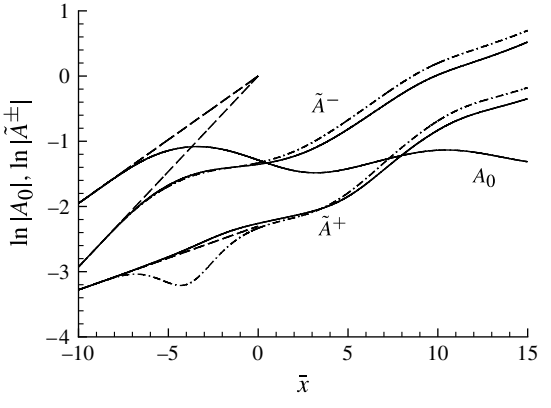

FIGURE 5. Development of the central mode and sideband perturbations for a small Haberman parameter $\bar{\lambda} = 1.54 \times 10^{-3}$: solid lines, $\varphi_0 = \pi$; dash-dotted lines, $\varphi_0 = \pi/2$.

Calculations are also performed for a Haberman parameter that is a tenth of that corresponding to the experimental condition of Miksad (1973). The development of the centre mode and sideband perturbations is displayed in figure 5. Clearly, the qualitative

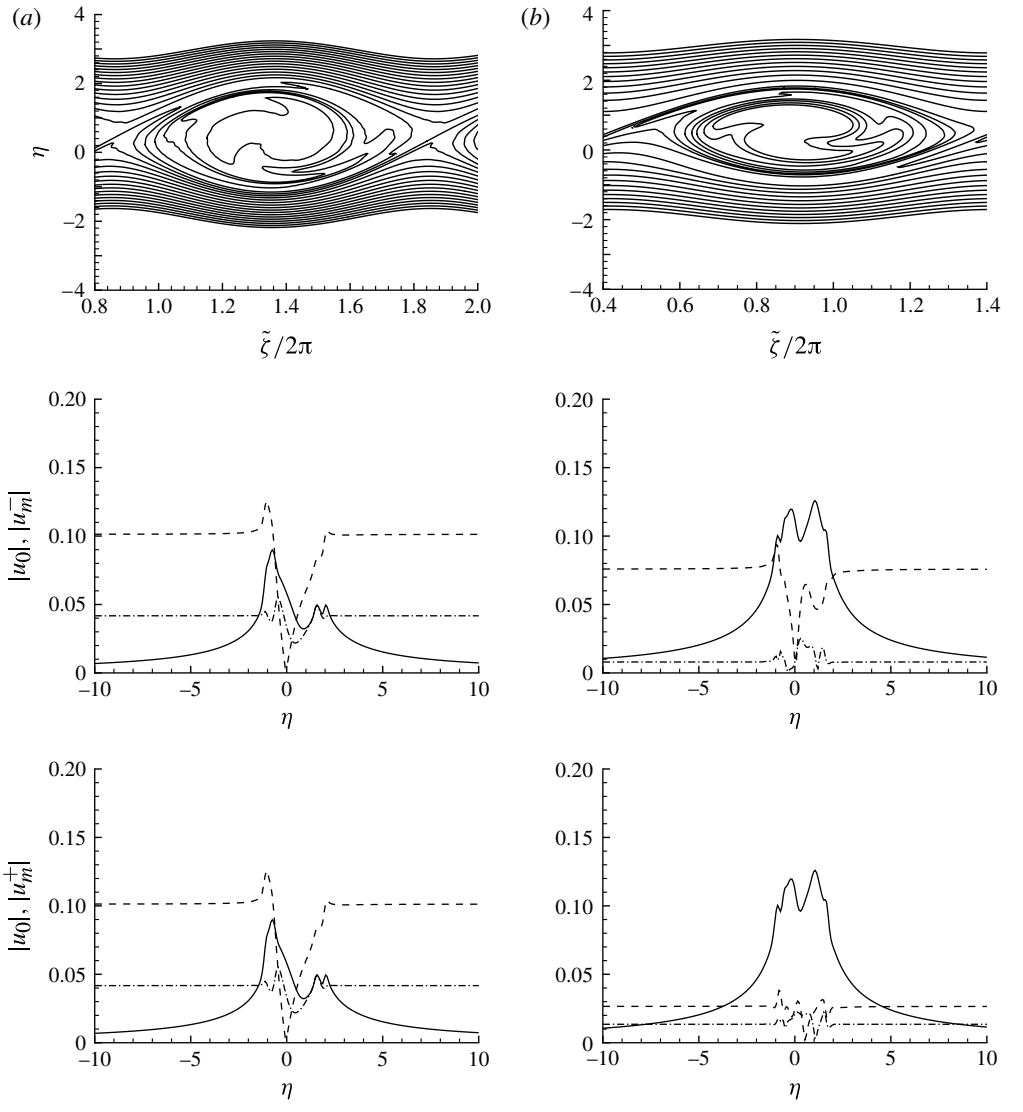

FIGURE 6. Contours of the critical-layer vorticity $\Omega_{0,c}$ of the central mode and profiles $u_m^{\pm}$ (see (5.11)) of sideband components ($m\omega_0 \pm \omega_\nu$) for $\bar{\lambda} = 1.54 \times 10^{-3}$ at (*a*) $x = -2$ and (*b*) 5. Solid lines, difference-frequency component $|u_0|$; dashed lines, $|u_2^{\pm}|$; dash-dotted lines, $|u_3^{\pm}|$.

feature is the same as shown in figure 1, that is, the sideband interaction promotes the amplification of $\omega_0 + \omega_\nu$ but inhibits $\omega_0 - \omega_\nu$. Compared with the regular cat's eye structure, the vorticity field of the central mode rolls up to form a much more complicated pattern (figure 6). The result in the figure indicates that the sideband interaction generates a significant level of difference-frequency component ω_ν and lower-band component $2\omega_0 - \omega_\nu$.

The fully nonlinear system (3.25) is solved for the (scaled) initial amplitudes $a_0 = 1$, $a_0^- = 0.3$ (an estimate based on the data in figure 7 of Miksad (1973)), $a_0^+ = 0.03$ and the phase difference $\varphi_0 = \pi$, where a very small a_0^+ was specified in order to

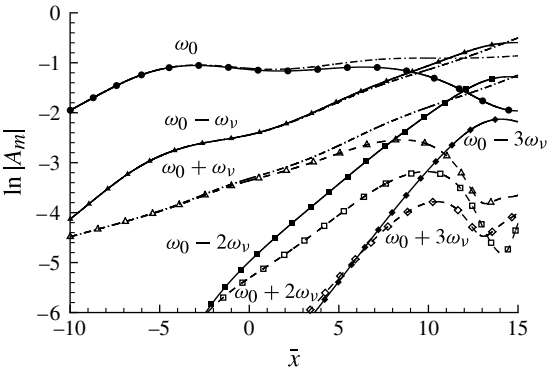

FIGURE 7. Development of A_m, the amplitudes of components $\omega_0 \pm m\omega_\nu$ ($m = 0, 1, 2, 3$). Solid line with squares, $\omega_0 - 2\omega_\nu$; solid line with diamonds, $\omega_0 - 3\omega_\nu$; dashed line with squares, $\omega_0 + 2\omega_\nu$; dashed line with diamonds, $\omega_0 + 3\omega_\nu$. The dash-dotted lines represent the prediction of the linear sideband analysis ($\varphi_0 = \pi$).

mimic the two-mode excitation by ω_0 and $\omega_0 - \omega_\nu$. The development of A_m is shown in figure 7. In the initial stage, the central mode ω_0 evolves primarily under the influence of its own nonlinearity, but it inhibits $\omega_0 - \omega_\nu$ and promotes $\omega_0 + \omega_\nu$. The latter two seeded modes follow the prediction of linear sideband instability analysis, indicating that their back action is negligible despite that mode $\omega_0 - \omega_\nu$ has a finite amplitude $\sim 1/3$ of that of ω_0 mode. The fully nonlinear stage commences from $\bar{x} \approx 2$. The back action comes into play, inhibiting ω_0 and $\omega_0 + \omega_\nu$ modes and eventually causing them to decay. The $\omega_0 - \omega_\nu$ mode, however, continues to grow and overtakes the central mode by $\bar{x} \approx 8.5$; it is little affected by the back action until $\bar{x} \approx 10$. The overall behaviour of ω_0 and $\omega_0 \pm \omega_\nu$ modes is quite similar to that shown in figure 7 of Miksad (1973). The fully nonlinear interaction generates components $\omega_0 \pm 2\omega_\nu$, $\omega_0 \pm 3\omega_\nu$, etc., leading to broadening of the spectral band centred at ω_0. While $\omega_0 + 2\omega_\nu$ and $\omega_0 + 3\omega_\nu$ initially have somewhat larger amplitudes than those of $\omega_0 - 2\omega_\nu$ and $\omega_0 - 3\omega_\nu$ modes, it is the latter that amplify over a longer distance to gain amplitudes comparable with that of the central mode. Within the sideband of ω_0, there seems to be a local cascade of energy towards lower-frequency components. A similar process occurs among the components in the band centred at $2\omega_0$ as shown in figure 8(a). The first harmonic $2\omega_0$ initially has a larger amplitude, but it is overtaken by $2\omega_0 - \omega_\nu$ when $\bar{x} \approx 4$. The latter is surpassed by $2\omega_0 - 2\omega_\nu$ at $\bar{x} \approx 13$. This general trend is in qualitative agreement with the measurements of Miksad (1973). We have also performed the calculation for $a^+ = 0$, but the results are not presented since they are close to what is shown above (except that the upper-band component, being forced by nonlinear interactions, has a very small amplitude in the earlier stage of the evolution).

In addition to the local cascade, a non-local cascade appears to take place, namely, interactions of components within the sideband of $n\omega_0$ generate components $m\omega_\nu$ in the low-frequency band. Figure 8(b) shows the development of $u_0^{(m)}$, the maximum streamwise velocity of these components. Among these the mean-flow distortion $\omega = 0$ is the strongest. The difference-frequency mode is also significant, consistent with the experimental observation of Miksad (1973).

When the shear layer is excited by a disturbance consisting of two frequencies, the vorticity field is modulated slowly on the time scale $2\pi/\omega_\nu$. For the present form of

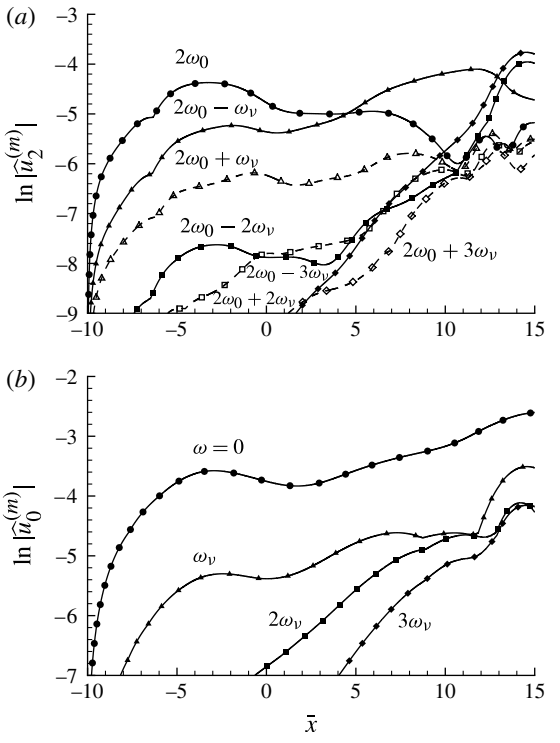

FIGURE 8. Development of (*a*) the maximum streamwise velocity $\widehat{u}_2^{(m)}$ of the first harmonic $2\omega_0$ and the sideband components $2\omega_0 \pm m\omega_\nu$, and (*b*) the maximum streamwise velocity $\widehat{u}_0^{(m)}$ of the mean-flow distortion ($m = 0$) and the low-frequency sideband components $m\omega_\nu$ ($m = 1, 2, 3$). (*a*) Solid line with squares, $2\omega_0 - 2\omega_\nu$; solid line with diamonds, $2\omega_0 - 3\omega_\nu$; dashed line with squares, $2\omega_0 + 2\omega_\nu$; dashed line with diamonds, $2\omega_0 + 3\omega_\nu$.

disturbance, the modulation is periodic in τ with a period $T = 2\pi/\Delta$. In figure 9, vorticity contours at the streamwise location $\bar{x} = 15$ are displayed for different instants $\tau = 0$, $0.25T$, $0.5T$ and $0.75T$. The vorticity is somewhat redistributed during the modulation cycle, but the roller retains its topological feature. Figure 10 shows the streamwise velocity profiles $\widehat{u}_0^{(n)}$ of low-frequency components $n\omega_\nu$ ($n = 1, 2, 3$) and the mean-flow distortion ($n = 0$). They have different distributions at $\bar{x} = 10$, but farther downstream (e.g. $\bar{x} = 15$) they acquire a broadly similar shape with two peaks above and below the critical level. The mean-flow distortion is clearly dominant, but the non-zero frequency components reach a significant level. Profiles of sideband components of the first harmonic $2\omega_0$, are also displayed in figure 10. At $\bar{x} = 10$, the lower-band component $2\omega_0 - \omega_\nu$ is much stronger than the first harmonic. At $\bar{x} = 15$, a range of lower-band components $2\omega_0 - m\omega_\nu$ ($m = 1, 2, 3$) have overtaken $2\omega_0$. Upper-band modes $2\omega_0 + m\omega_\nu$ ($m > 0$) have amplified too but are weaker than the first harmonic. It is interesting to note that the lower-band components $2\omega_0 - m\omega_\nu$ have larger amplitudes than the upper-band components $2\omega_0 + m\omega_\nu$, an indication of local 'back scattering', i.e. energy cascade into lower-frequency modes.

The discrete spectrum $\widehat{u}(\omega)$ of the streamwise velocity at the critical level follows from the Fourier representation (5.6). Figure 11 shows the evolution of $\widehat{u}(\omega)$. When $\bar{x} = 0$, the spectrum consists of well-defined peaks at the fundamental and harmonic

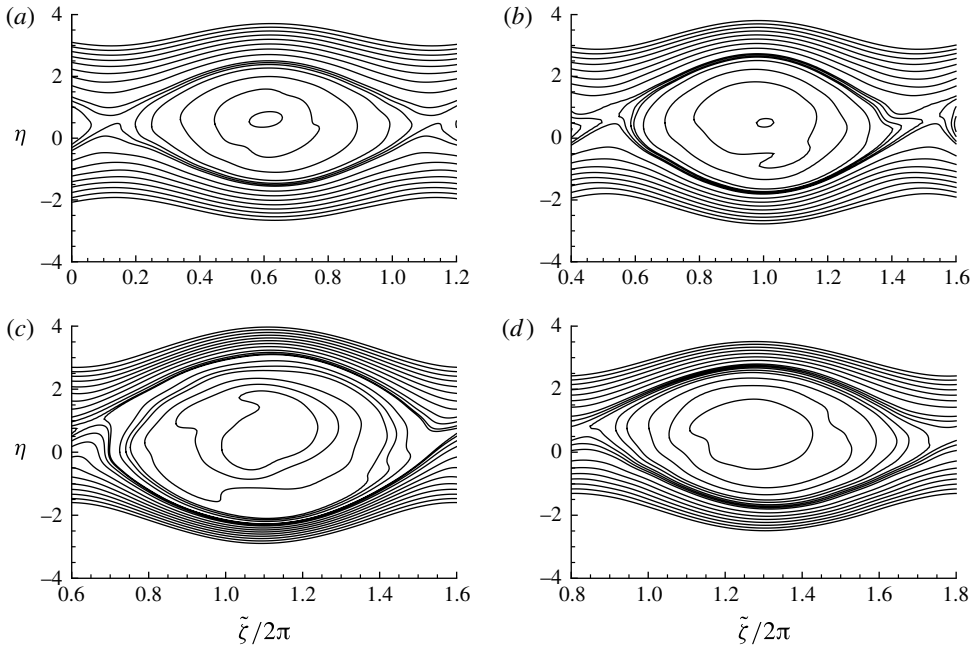

FIGURE 9. Contours of the critical-layer vorticity Ω_c at $\bar{x} = 15$ and $\tau = 0, 0.25T, 0.5T$ and $0.75T$.

frequencies. The low-frequency components are already significant, as indicated by the peak centred at $\omega = 0$. As $\bar{x}$ increases (e.g. $\bar{x} = 5$), the width of each peak widens, and the 'troughs' between the peaks are gradually filled up due to interactions of low-frequency components with the fundamental and harmonic components. By $\bar{x} = 15$, only the peaks at zero and the fundamental frequencies remain discernable while those at harmonics have almost disappeared. The corresponding time traces at these locations are displayed in figure 12. To aid the interpretation, we extract the real amplitude a and phase p by writing the complex amplitude function as $A = ae^{ip}$. The modulation of the phase, p', represents the frequency shift. Modulations of a, p and p' are displayed in figure 12(b). At $\bar{x} = 0$, the disturbance exhibits the character of a wavepacket, with its envelope and phase modulated gradually on the time scale of $2\pi/\omega_v$. The modulation becomes more abrupt and intermittent as the wavetrain propagates downstream (e.g. at $\bar{x} = 5$). Interestingly, between the two consecutive modulations, the amplitude and the frequency shift remain almost constant. At $\bar{x} = 13$, oscillations occur between the abrupt adjustments, and correspondingly the time signal appears quite 'irregular' or 'chaotic'. The result indicates that spectral broadening is indeed associated with amplitude and phase modulations as was suggested by experimentalists.

5.2. *Planar wake*

For the case of a planar wake, calculations will be performed for the profile

$$\bar{U} = U_0 - \operatorname{sech}^2 y, \tag{5.12}$$

where U_0 is the free-stream velocity normalized by the deficit velocity. Two types of modes, sinuous and varicose, exist, and they may interact nonlinearly (Leib &

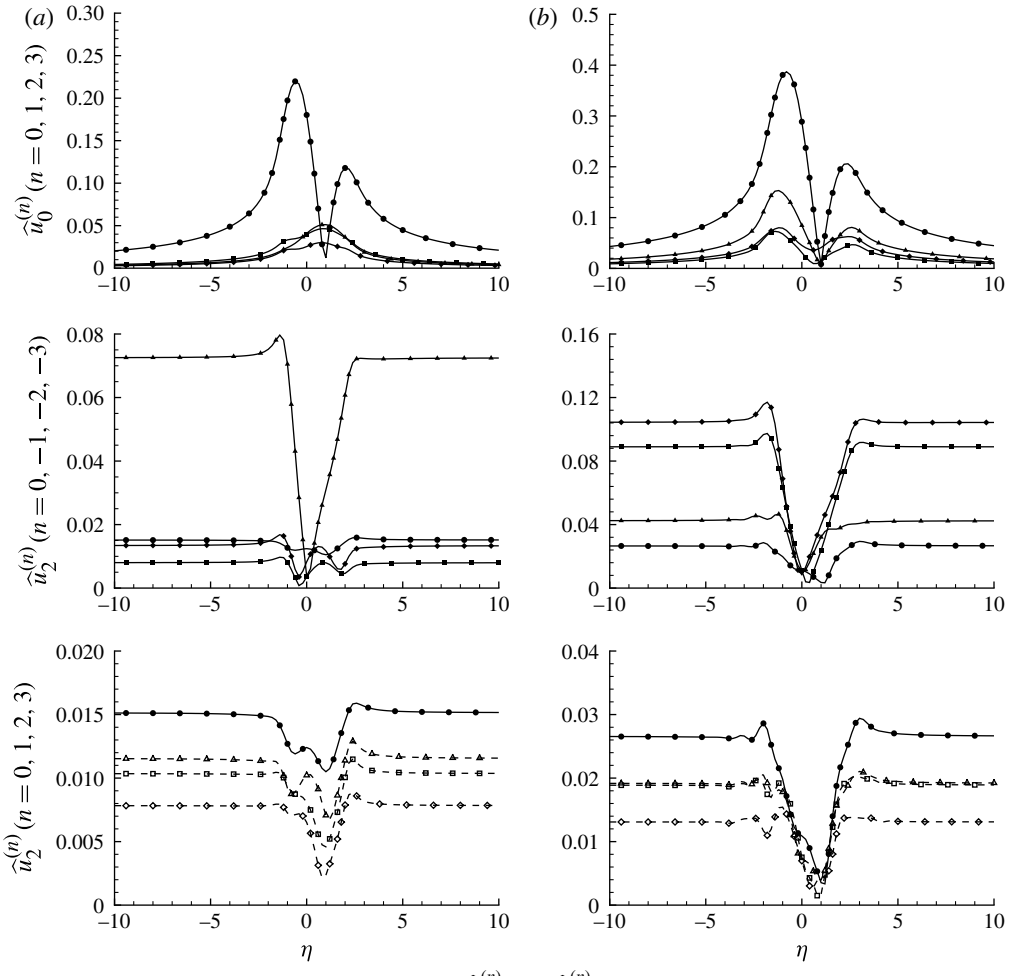

FIGURE 10. Streamwise velocity profiles, $\widehat{u}_0^{(n)}$ and $\widehat{u}_2^{(n)}$, of the components $n\omega_v$ and $2\omega_0 + n\omega_v$ at (*a*) $\bar{x} = 10$ and (*b*) 15. Solid lines: dots, $n = 0$; squares, $n = -1$; triangles, $n = -2$; diamonds, $n = -3$. Dashed lines: squares, $n = 1$; triangles, $n = 2$; diamonds, $n = 3$.

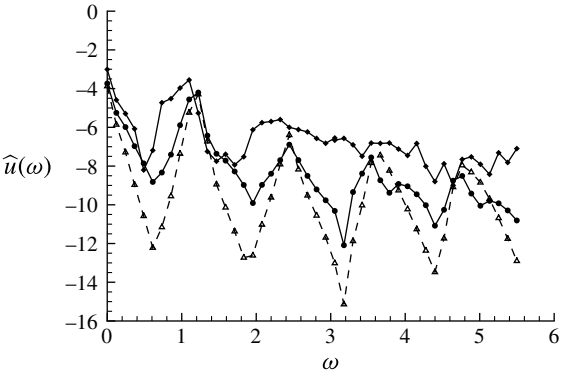

FIGURE 11. Spectrum of the streamwise velocity at three streamwise locations: dashed line with triangles, $\bar{x} = 0$; solid line with dots, $\bar{x} = 5$; solid line with diamonds, $\bar{x} = 13$.

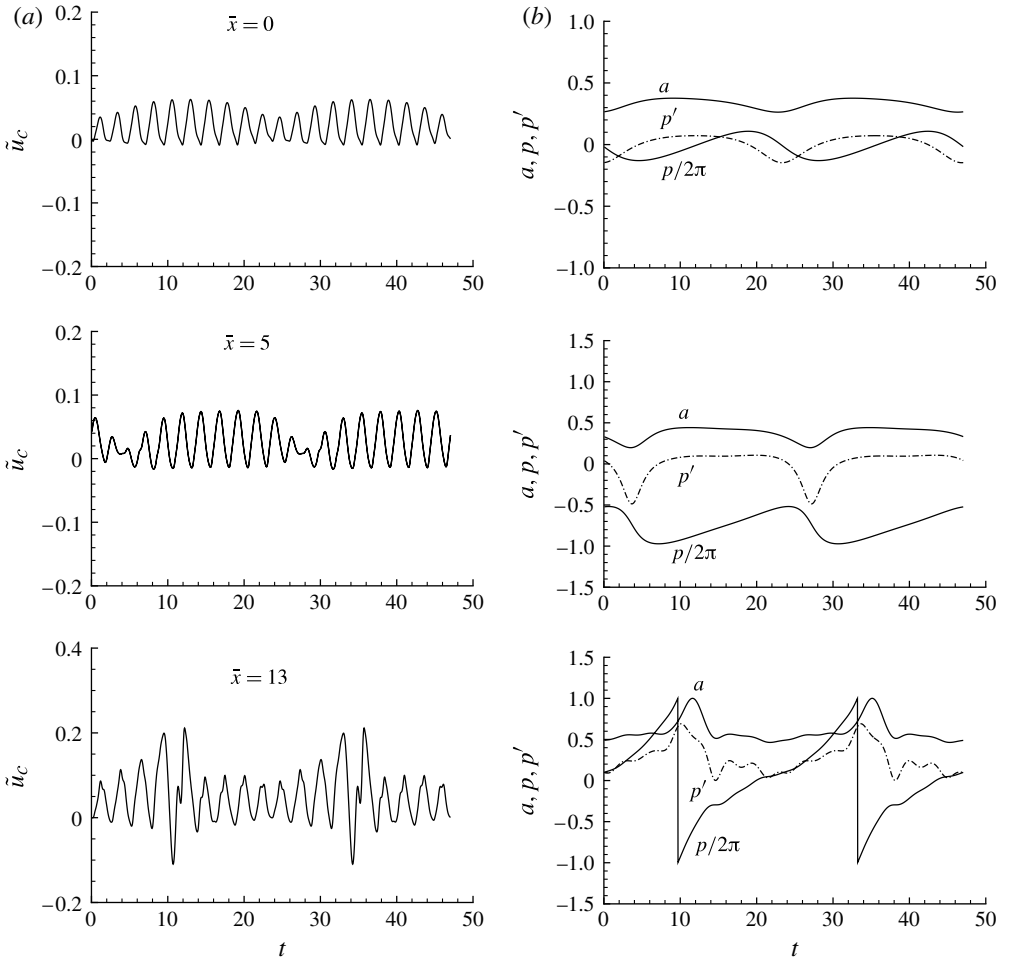

FIGURE 12. (*a*) Time trace of $\tilde{u}_c$, the instantaneous streamwise velocity at the critical level, and (*b*) amplitude–phase modulations at $\bar{x}=0$, 5 and 13.

Goldstein 1989; Wu 1996). We shall consider only sinuous modes, which represent the dominant instability. For the neutral mode,

$$\alpha=2, \quad c=U_0-\frac{2}{3}, \quad \phi=\frac{3}{2}\mathrm{sech}^2 y, \quad J_1=3, \quad J_2=18\left[\frac{1}{\sqrt{3}}\ln(2+\sqrt{3})+2\right]. \tag{5.13}$$

The two critical layers are located at $y_c^{\pm}=\pm(1/2)\ln(2+\sqrt{3})$, and

$$U'(y_c^+)=-U'(y_c^-)=4\sqrt{3}/9, \quad U'''(y_c^+)=-U'''(y_c^-)=-16\sqrt{3}/9. \tag{5.14}$$

The vorticity $Q_n^{\pm}$ in the upper and lower critical layers is governed by nonlinear evolution equations like (3.12). It may be inferred by an inspection of the equations that $Q_n^{\pm}$ is symmetric/antisymmetric if n is odd/even. By using this symmetry, it suffices to solve the equations for Q_n^{+} only. The amplitude equation remains the same

as (3.19) provided that the coefficients are replaced by

$$\tilde{\Lambda}_1 = \left(\Lambda_1 - \frac{4\mathrm{i}S_0}{H}\right) q - 4\left[4 - \frac{\mathrm{i}S_0\Lambda_1}{H} + \frac{16\mathrm{i}S_0}{H\Lambda_2}\right] + \frac{4\mathrm{i}S_0\Lambda_1\Lambda_d}{H\Lambda_2}, \tag{5.15a}$$

$$\tilde{\Lambda}_2 = \left(\Lambda_2 - \frac{4\mathrm{i}S_0}{H}\right) q - 4\left[4 - \frac{\mathrm{i}S_0\Lambda_1}{H} + \frac{16\mathrm{i}S_0}{\Lambda_2 H}\right], \tag{5.15b}$$

$$\tilde{\Lambda}_{d,j} = \frac{4\Lambda_d}{H}\left[1 - \frac{4\mathrm{i}S_0}{H\Lambda_2} + \frac{\Lambda_j}{\Lambda_2}\right] \quad (j = 1, 2), \quad \tilde{\Lambda}_0 = -\mathrm{i}S_0\Lambda_1 q + 16\mathrm{i}S_0, \tag{5.15c}$$

$$q = \Lambda_2 - \frac{4\mathrm{i}S_0}{H} - \frac{16}{\Lambda_2} + \frac{4\mathrm{i}S_0\Lambda_1}{H\Lambda_2}. \tag{5.15d}$$

The symmetry property of $Q_n^{\pm}$ implies that the streamwise velocity of the even/odd order harmonics would be symmetric/antisymmetric respectively, consistent with the observation of Sato & Saito (1975).

The harmonic components in the main layer have to be found numerically. This can be done most efficiently by introducing functions $h_m(y)$, which are defined by the boundary-value problem consisting of the homogeneous Rayleigh equation

$$\mathscr{L}(m\alpha)h_m = 0, \tag{5.16}$$

and the jump and boundary conditions

$$h_m(y_c^+) - h_m(y_c^-) = 0, \quad h_m'(y_c^+) - h_m'(y_c^-) = 1, \tag{5.17}$$

$$h_m(0) = 0 \quad (\text{for even } m), \quad h_m'(0) = 0 \quad (\text{for odd } m), \quad h_m \to 0 \quad \text{as } y \to \infty; \tag{5.18}$$

here we have used the fact that h_m are symmetric/antisymmetric with respect to y for odd/even $m \geqslant 2$ because Q_m are. Now that h_m are independent of $\bar{x}$ and τ, they can be computed once for all. The solution for $\phi_2^{(m)}$ can then be written as

$$\phi_2^{(m)}(y, \bar{x}, \tau) = J_m(\bar{x}, \tau)h_m(y), \tag{5.19}$$

which is of variable separation form. Clearly, the shape of harmonic components in the main layer, characterized by $h_m(y)$, remains unchanged during the evolution. However, the distribution within the critical layer is continuously distorted because of the combined nonlinear and non-equilibrium effects.

The solution for $\phi_2^{(1)}$ is given by (2.21) with $C^+ = 0$, but the constant C^- must instead be determined by the symmetric condition about $y = 0$, which leads to a value half that given by (2.23). The streamwise velocity at an arbitrary position $y \neq y_c^{\pm}$ is found as

$$\tilde{u} = \epsilon A^{\dagger}\phi_1' \mathrm{e}^{\mathrm{i}\tilde{\zeta}} + \epsilon^{3/2}\left\{\phi_2^{(1)\prime}\mathrm{e}^{\mathrm{i}\tilde{\zeta}} + \sum_{m=2} h_m'(y)J_m(\bar{x}, \tau)\mathrm{e}^{\mathrm{i}m\tilde{\zeta}}\right\} + \text{c.c.} \tag{5.20}$$

For the planar-wake profile (5.12), $a_1 = -2/\sqrt{3} \neq 0$ and so it follows from (5.3)–(5.5) and (5.6) that $\tilde{u}_c$, the total streamwise velocity of the perturbation within the critical layer, is dominated by the fundamental to leading order, with harmonic contents contributing an $O(\epsilon^{1/2})$ correction. In fact, the streamwise velocity of the leading-order fundamental attains its maximum at the critical level, in contrast to the case of a mixing layer, for which the same quantity vanishes at y_c (i.e. $a_1 = 0$). Therefore $\tilde{u}_c$ would exhibit less temporal complexity in a planar wake than in a mixing layer. This expectation is consistent with experimental data (shown for example in figures 5 and 7 of Miksad *et al.* 1982), and will be confirmed by our numerical

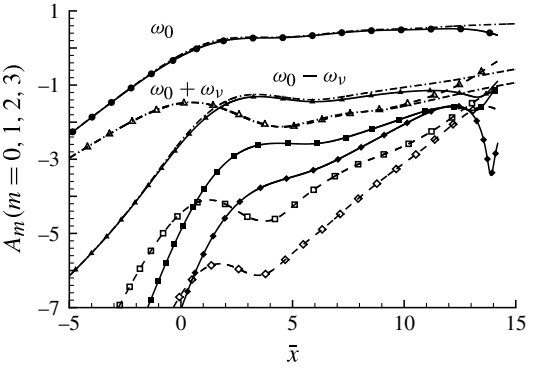

FIGURE 13. Development of A_m, the amplitudes of components $\omega_0 \pm m\omega_\nu$ ($m = 0, 1, 2, 3$). Solid line with squares, $\omega_0 - 2\omega_\nu$; solid line with diamonds, $\omega_0 - 3\omega_\nu$; dashed line with squares, $\omega_0 + 2\omega_\nu$; dashed line with diamonds, $\omega_0 + 3\omega_\nu$. The dash-dotted lines represent the prediction of the linear sideband analysis ($\varphi_0 = \pi$).

calculations. Equation (5.5) and (5.20) indicate that in order to obtain the velocity of the perturbation to $O(\epsilon^{1/2})$ accuracy, it is necessary to compute B by solving the system (B 4)–(B 5).

The values of the parameters for the calculation were chosen to mimic the experiments of Miksad *et al.* (1982). The central mean velocity is taken to be $0.6U_\infty$, and the Reynolds number based on the wake half-width and the free-stream velocity U_∞ is 1575, which corresponds to $R = 714$ for the profile and the normalization adopted in the present paper. The root-mean-square value of $0.08U_\infty$ was used as a reference to set the disturbance amplitude $\epsilon = 0.122$ and accordingly a Haberman parameter $\bar{\lambda} \approx 0.077$. Unlike the mixing-layer experiments (Miksad 1973), the frequencies of the two seeded modes differ only by 5.5 %. In our calculations, we take the central mode frequency $\omega_0 = 0.8\alpha c$, i.e. $\epsilon^{1/2} S_0 = \alpha c/5$, and set $\omega_\nu = \alpha c/20$, which gives a 6.7 % frequency difference, very close to the experimental value. The initial condition corresponds to $a_0 = 1$, $a_0^+ = 1/3$ and $a_0^- = 1/30$ to approximate a forced two-frequency excitation by ω_0 and ω^+. It should be pointed out that differences still exist between the calculation and the laboratory condition: the experiments investigated the disturbance development in the region fairly close to the trailing edge, where the mean flow differs from (5.12), and the Reynolds number in the experiments is quite low. Nevertheless, we believe that key physical mechanisms are captured, at least qualitatively, by the present theory.

Figure 13 shows the development of the amplitudes of sideband components $\omega_0 \pm m\omega_\nu$ ($m = 1, 2, 3$) including the central mode ω_0. Similar to the mixing-layer case, of the main two seeded modes the one with a larger amplitude (i.e. the central mode ω_0) suppresses the mode with a smaller amplitude, which is $\omega_0 + \omega_\nu$ in the present case. The lower-band component $\omega_0 - \omega_\nu$ is promoted initially by the sideband interaction, and grows rather rapidly to exceed the amplitude of the seeded upper-band mode $\omega_0 + \omega_\nu$. Both modes eventually attenuate. Comparison with the prediction of linear sideband instability indicates that the nonlinearity of $\omega_0 \pm \omega_\nu$ modes hardly affects the evolution of themselves or the central mode ω_0. However, when all self and mutual nonlinear effects are included, further sideband components, $\omega_0 \pm m\omega_\nu$, $2\omega_0 \pm m\omega_\nu$, etc., are generated. Lower-band components $\omega_0 - m\omega_\nu$ evolve to acquire larger amplitudes than those of upper-band modes, $\omega_0 + m\omega_\nu$ ($m = 2, 3$). Figure 14(*a*)

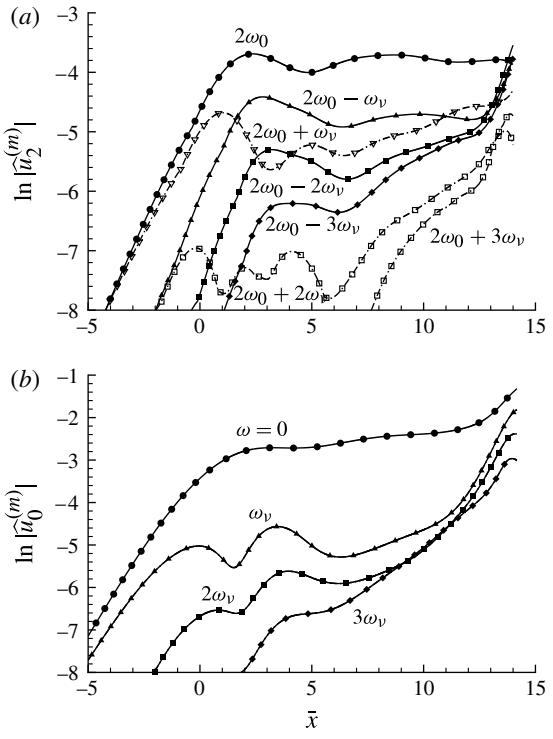

FIGURE 14. Development of (*a*) the maximum streamwise velocity $\widehat{u}_2^{(m)}$ of the first harmonic $2\omega_0$ and the sideband components $2\omega_0 \pm m\omega_\nu$, and (*b*) the maximum streamwise velocity $\widehat{u}_0^{(m)}$ of the mean-flow distortion ($m = 0$) and the low-frequency sideband components $m\omega_\nu$ ($m = 1, 2, 3$). (*a*) Solid line with squares, $2\omega_0 - 2\omega_\nu$; solid line with diamonds, $2\omega_0 - 3\omega_\nu$; dashed line with squares, $2\omega_0 + 2\omega_\nu$; dashed line with diamonds, $2\omega_0 + 3\omega_\nu$.

shows the evolution of the first harmonic $2\omega_0$ and its sideband components $2\omega_0 \pm m\omega_\nu$. The lower-band components are much stronger than their corresponding upper-band counterparts. A strong mean-flow distortion and low-frequency components $m\omega_\nu$ are generated, as indicated by figure 14(*b*).

The evolution of the spectrum of the streamwise velocity at the critical level is shown in figure 15. For $3 \leqslant \bar{x} \leqslant 12$, the fundamental and harmonics have almost saturated, but their sideband components amplify to fill in the spectral gaps between the harmonics. The mean-flow and low-frequency components do not appear prominent in this plot. This is because their amplitudes happen to reach local minima near $\eta = 0$. Though not shown, the spectrum at $\eta = 5$ features a clear peak centred at zero frequency as well as those at the fundamental and harmonics. The spectral broadening process is qualitatively similar to the measurements presented in figure 6 of Miksad *et al.* (1982).

Figure 16 shows the time series and the amplitude–phase modulation. At $\bar{x} = 3$, both the amplitude a and phase p are modulated slowly, leading to a smooth frequency shift p'. The corresponding time trace appears as a modulated wavetrain. At downstream locations (e.g. $\bar{x} = 8$) the modulation becomes more intermittent and abrupt, and in between the two consecutive modulations the amplitude and frequency remain almost constant so that the time trace appears almost as a monochromatic

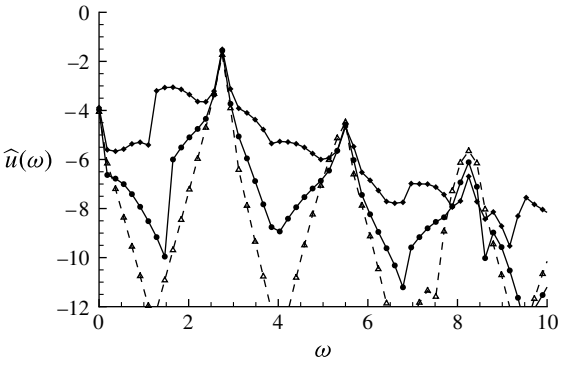

FIGURE 15. Spectrum of the streamwise velocity at three streamwise locations: dashed line with triangles, $\bar{x} = 3$; solid line with dots, $\bar{x} = 8$; solid line with diamonds, $\bar{x} = 12$.

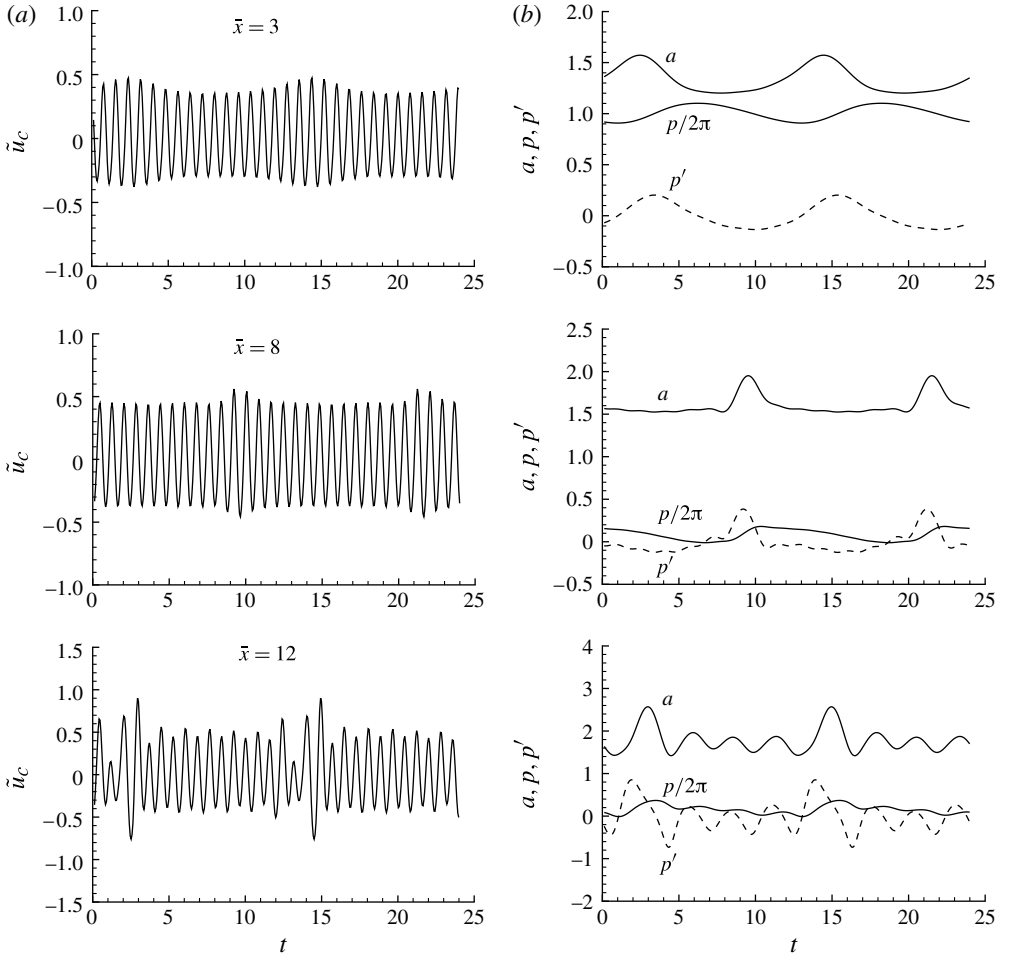

FIGURE 16. (*a*) Time trace of $\tilde{u}_c$, the instantaneous streamwise velocity at the critical level, and (*b*) amplitude–phase modulations at $\bar{x} = 3$, 8 and 12.

wave. Farther downstream, several oscillations occur between the major modulations, and accordingly the time-domain signal becomes less regular. The amplitude–phase modulation is very similar to that occurring in a mixing layer (see figure 12). However, for the reason explained earlier, the time signature is not as 'chaotic'. The predicted characteristics of time traces and the amplitude–phase modulation as well as their evolution sequence are in good qualitative agreement with the experimental data presented in figures 5–7 of Miksad *et al.* (1982), suggesting that the present theory captures the key physical mechanisms involved.

6. Summary and conclusions

The present theoretical work is intended to offer a theoretical explanation for experimental observations concerning nonlinear dynamics of a free shear layer when it is excited by a disturbance consisting of two waves with nearly equal frequencies, ω_0 and ω_1. Since the frequency difference $\omega_\nu = \omega_0 - \omega_1$ is typically small, one wave is a sideband component of the other, and a dynamical model was therefore proposed, in which the disturbance is represented by a wavetrain, which is spatially and temporally modulated on the (non-dimensional) length and time scales of order ω_ν^{-1}. This is a more general form of disturbance since it has a continuous sideband spectrum containing the two waves. The evolution system governing the nonlinear development of the wavetrain is derived by using the nonlinear, non-equilibrium critical layer approach. In the special case of a single-frequency disturbance, the system reduces to that derived by Goldstein & Leib (1988) and Goldstein & Hultgren (1988), and as has been shown by these authors, the dominant instability wave saturates, and the vorticity field rolls up to form the distinctive pattern of 'rollers'. In order to shed light on the nonlinear dynamics in the presence of two-frequency excitation, we first consider the linear instability of the dominant wave (with frequency ω_0) to sideband perturbations with frequencies $\omega_0 \pm \omega_\nu$. Compared with the conventional sideband instability of an equilibrium wave, which is usually governed by an eigenvalue problem and destabilizes both sideband components, the sideband instability in the present context exhibits quite different features. As the base wave is spatially evolving, the sideband instability must be formulated as an initial-value problem. The latter is governed by a parametrically excited system because the vorticity 'roller' is strongly nonlinear. Numerical solutions indicate that due to the non-equilibrium effect, evolution of the sideband perturbations may exhibit rather complex transient behaviours depending on their phase relation and initial amplitude ratio. When the ratio differs appreciably from unity, the base (central) wave suppresses the stronger one of the two sideband modes, but may enhance the other; when the initial amplitude ratio is of $O(1)$, both sideband modes are inhibited. However, regardless of the amplitude ratio, the two sideband modes would eventually amplify at a synchronized rate, which turns out to be between their linear growth rates, and the lower-band perturbation always evolves to acquire a larger amplitude. The sideband interaction leads to generation of a strong difference-frequency mode ω_ν, and because of parametric excitation, sideband components $m\omega_0 \pm \omega_\nu$ $(m = 0, 1, 2, \ldots)$ are generated too. Precisely owing to these unique features, the present sideband interaction can explain the seemingly conflicting observations: the 'suppressing' effect and the appearance of sideband components, which cannot be explained by the conventional sideband instability.

The nonlinear evolution system is solved numerically for the case where the perturbation consists of two modes with comparable magnitudes. Two types of shear layers were considered: a mixing layer and a planar wake, and the results turned out

to be broadly similar. The central mode ω_0 and its sideband components $\omega_0 + n\omega_v$ are most dominant. Due to strongly nonlinear effects within the critical layer, components with the combination frequencies $m\omega_0 + n\omega_v$ ($m \geqslant 2$) are generated simultaneously at the same order. As the disturbance evolves downstream, low-frequency fluctuations $n\omega_v$ and the mean-flow distortion attain quite large amplitudes, and so do the harmonics $m\omega_0$ ($m \geqslant 2$) and the sideband components in their vicinities. The spectrum of the disturbance therefore broadens progressively, and the corresponding time trace of the perturbation appears to be increasingly irregular. Within each sideband of $m\omega_0$, the components in the lower-band ($n < 0$) become stronger than those in the upper band ($n > 0$). This may be an indication of local inverse energy cascade or 'back scattering', whereas the occurrence of large low-frequency components is suggestive of a global energy cascade. These theoretical results are broadly in agreement with experimental measurements.

It was pointed out by Sato (1970) and Miksad *et al.* (1982) that much of the observed temporal dynamics of the disturbance, especially the spectral broadening, was associated with simultaneous amplitude and phase modulations over the time scale of order $2\pi/\omega_v$. Measurements of bi-coherency spectrum by Miksad *et al.* (1982) and Ritz *et al.* (1988) indicate that dominant nonlinear interactions contributing to the modulations include (i) the self-interaction of ω_0, generating harmonics $m\omega_0$, (ii) the mutual interaction between ω_0 and ω_1, which produces the difference mode ω_v, and (iii) further interactions between ω_v and $m\omega_0$ to generate $m\omega_0 + n\omega_v$. A dynamical model based on first principles was, however, not available. The present work provides precisely such a model, which accounts for those interactions. The predicted amplitude and phase modulations exhibit characteristics similar to experimental observations (Miksad *et al.* 1982).

In the last two decades or so, the method of parabolized stability equations (PSE) (Herbert 1997) has emerged as an effective tool to predict linear and nonlinear development of instability modes in nearly parallel shear flows, including free shear layers; e.g. Sandham & Salgado (2008), Cheung & Lele (2009), and references therein. This approach has, to some extent, taken over the role of (weakly) nonlinear instability theory. The crucial approximation, parabolization, is made on the assumption that the shape of the disturbance evolves slowly so that a local wavenumber may be defined. However, short of specifying the distinct scales unambiguously, the wavenumber has to be determined in a rather *ad hoc* manner. The step size of marching for solving the resultant PSE cannot be refined indefinitely. In contrast, the present nonlinear critical layer theory is a completely self-consistent asymptotic formulation with clearly defined scales. It leads to a parabolized system, which imposes no lower limit on permissible step size. The theory has been adapted to nonlinearly modulated wavetrains/packets, whereas the PSE approach has, to the best of our knowledge, been restricted to sinusoidal disturbances consisting of a single frequency or frequencies satisfying harmonic relations. Therefore, not only will nonlinear critical layer theory itself remain an important tool, but hopefully it may also stimulate further developments of the PSE methodology, such as finding a better way to define the local wavenumber and broadening its scope of application (e.g. to wavepackets).

As mentioned in § 1, lower-frequency components may radiate a significant amount of noise in subsonic jets. Work is in progress to develop a first-principles theory for predicting the far-field acoustic field.

Acknowledgement

We would like to thank the referees for their helpful comments and suggestions.

Appendix A. Derivation of (3.19)

Let $\mathscr{D}_0 = ((\partial/\partial\tau) + (\partial/\partial\bar{x}))$ act on both sides of (3.17) with the $O(1/M)$ terms omitted. Then

$$\left(-\mathrm{i}S_0\Lambda_1 + \Lambda_1\frac{\partial}{\partial\tau} + \Lambda_2\frac{\partial}{\partial\bar{x}}\right)\mathscr{D}_0 A = \int_{-H}^{H}\mathscr{D}_0 Q_1\,\mathrm{d}\eta$$
$$= -2H(\mathscr{D}_0 - \mathrm{i}S_0)A - \mathrm{i}I_{11} + O(H^{-1}), \quad (A\,1)$$

where use has been made of (3.12) and (3.14). The above equation may be rewritten as

$$\Lambda_2\mathscr{D}_0^2 A = -\left(-\mathrm{i}S_0\Lambda_1 + \Lambda_d\frac{\partial}{\partial\tau}\right)\mathscr{D}_0 A - 2H(\mathscr{D}_0 - \mathrm{i}S_0)A - \mathrm{i}I_{11} + O(H^{-1}), \quad (A\,2)$$

where we have put $\Lambda_d = \Lambda_1 - \Lambda_2$. Using (A 2) in (3.17) to eliminate $\mathscr{D}_0^2 A$, we have

$$-\mathrm{i}S_0\Lambda_1 A + \Lambda_1\frac{\partial A}{\partial\tau} + \Lambda_2\frac{\partial A}{\partial\bar{x}} = I_{10} + \frac{2\mathrm{i}S_0}{H}\mathscr{D}_0 A + \frac{2}{H\Lambda_2}\left(-\mathrm{i}S_0\Lambda_1 + \Lambda_d\frac{\partial}{\partial\tau}\right)\mathscr{D}_0 A$$
$$+ \frac{4}{\Lambda_2}(\mathscr{D}_0 - \mathrm{i}S_0)A + \frac{2\mathrm{i}I_{11}}{H\Lambda_2} + O(H^{-2}), \quad (A\,3)$$

which may be arranged to

$$\mathscr{D}_1\mathscr{D}_0 A = I_{10} - \left(-\mathrm{i}S_0\Lambda_1 + \Lambda_d\frac{\partial}{\partial\tau}\right)A - \frac{4\mathrm{i}S_0}{\Lambda_2}A + \frac{2\mathrm{i}I_{11}}{H\Lambda_2} + O(H^{-2}), \quad (A\,4)$$

where

$$\mathscr{D}_1 = \Lambda_2 - \frac{2\mathrm{i}S_0}{H} - \frac{4}{\Lambda_2} - \frac{2}{H\Lambda_2}\left(-\mathrm{i}S_0\Lambda_1 + \Lambda_d\frac{\partial}{\partial\tau}\right). \quad (A\,5)$$

Note that the equation (A 4) is first-order with respect to $\partial/\partial\bar{x}$, and the truncation error is $O(H^{-2})$.

Applying $\mathscr{D}_0$ to (A 4) again leads to

$$\mathscr{D}_1\mathscr{D}_0^2 A = -2H\left(\frac{\partial}{\partial\tau} + \frac{\partial}{\partial\bar{x}} - \mathrm{i}S_0\right)A - \mathrm{i}I_{11} - \left(-\mathrm{i}S_0\Lambda_1 + \Lambda_d\frac{\partial}{\partial\tau}\right)\mathscr{D}_0 A - \frac{4\mathrm{i}S_0}{\Lambda_2}\mathscr{D}_0 A$$
$$+ \frac{2\mathrm{i}}{H\Lambda_2}\left\{-\mathrm{i}I_{12} - \mathrm{i}\int_{-H}^{H}\eta\frac{\partial}{\partial\eta}(A^*Q_2 - AQ_0)\,\mathrm{d}\eta + O(H^{-1})\right\}$$
$$= \left\{-2H - \left(-\mathrm{i}S_0\Lambda_1 + \Lambda_d\frac{\partial}{\partial\tau}\right) - \frac{4\mathrm{i}S_0}{\Lambda_2}\right\}\mathscr{D}_0 A + 2H\mathrm{i}S_0 A - \mathrm{i}I_{11}$$
$$+ \frac{2}{H\Lambda_2}(I_{12} - A^*I_{20}) + O(H^{-2}). \quad (A\,6)$$

In the last step above, integration by parts is performed. Let $\mathscr{D}_1$ act on (3.17), and combine the resulting equation with (A 6) to eliminate the term $\mathscr{D}_0^2 A$. After rearranging, we finally obtain (3.19).

Appendix B. Evolution equations for B and Ω_3

In terms of the re-scaled variables

$$\Omega_3 = \Omega_3^{\dagger}\left(\alpha\bar{U}_c'\right)^2/\bar{U}_c''', \quad B = \alpha^2\bar{U}_c' B^{\dagger}\mathrm{e}^{\mathrm{i}S_0\tau}, \quad \widehat{b}_2^{(n)} = \alpha^2\bar{U}_c'\, b_2^{(n)}\mathrm{e}^{\mathrm{i}S_0\tau}, \tag{B 1}$$

the evolution system (2.44)–(2.45) may be rewritten as

$$\begin{aligned}\mathscr{L}_N\Omega_3 = &-\mathscr{D}_0\sum\widehat{b}_2^{(m)}\mathrm{e}^{\mathrm{i}m\tilde{\zeta}} - \frac{\mathrm{i}\chi_a}{\alpha\bar{U}_c'}\mathscr{D}_0^2 A\mathrm{e}^{\mathrm{i}\tilde{\zeta}} + \frac{1}{2}\frac{\bar{U}_c^{iv}}{\alpha\bar{U}_c'\bar{U}_c'''}(\mathrm{i}A^2\mathrm{e}^{2\mathrm{i}\tilde{\zeta}} + \text{c.c.}) + \text{c.c.}\\ &- (\alpha c)^{-1}(\eta + S_0)\frac{\partial\Omega}{\partial\bar{x}} - \frac{a_1}{\alpha\bar{U}_c'}(A\mathrm{e}^{\mathrm{i}\tilde{\zeta}} + \text{c.c.})\frac{\partial\Omega}{\partial\tilde{\zeta}}\\ &+ \left\{\sum_m \mathrm{i}m\widehat{b}_2^{(m)}\mathrm{e}^{m\mathrm{i}\tilde{\zeta}} + \left[\frac{\mathrm{i}a_1}{\alpha\bar{U}_c'}(\eta + S_0)A + (\alpha c)^{-1}\frac{\partial A}{\partial\bar{x}}\right]\mathrm{e}^{\mathrm{i}\tilde{\zeta}} + \text{c.c.}\right\}\frac{\partial\Omega}{\partial\eta}.\end{aligned} \tag{B 2}$$

The solution is expanded as a Fourier series

$$\Omega_3 = \sum_{n=-\infty}^{\infty}\widehat{\Omega}_n(\tau,\bar{x},\eta)\mathrm{e}^{\mathrm{i}n\tilde{\zeta}} \quad \text{with } \widehat{\Omega}_{-n} = \widehat{\Omega}_n^*. \tag{B 3}$$

Then $\widehat{\Omega}_n$ $(n = 0, 1, 2, \ldots)$ satisfies the equations

$$\begin{aligned}\mathscr{L}_{\mathscr{N}}\widehat{\Omega}_n = &-(\mathscr{D}_0 - n\mathrm{i}S_0)\widehat{b}_2^{(n)} - \delta_{1n}\frac{\mathrm{i}\chi_a}{\alpha\bar{U}_c'}(\mathscr{D}_0 - \mathrm{i}S_0)^2 A + \delta_{2n}\frac{1}{2}\frac{\bar{U}_c^{iv}}{\alpha\bar{U}_c'\bar{U}_c'''}(\mathrm{i}A^2)\\ &- (\alpha c)^{-1}(\eta + S_0)\frac{\partial Q_n}{\partial\bar{x}} + \sum_{m=1}^{\infty}\left(\mathrm{i}m\widehat{b}_2^{(m)}Q_{n-m,\eta} - \mathrm{i}m\widehat{b}_2^{(m)*}Q_{n+m,\eta}\right)\\ &- \frac{a_1}{\alpha\bar{U}_c'}\left[\mathrm{i}(n-1)AQ_{n-1} + \mathrm{i}(n+1)A^*Q_{n+1}\right]\\ &+ \left[\frac{\mathrm{i}a_1}{\alpha\bar{U}_c'}(\eta + S_0)A + (\alpha c)^{-1}\frac{\partial A}{\partial\bar{x}}\right]Q_{n-1,\eta}\\ &+ \left[-\frac{\mathrm{i}a_1}{\alpha\bar{U}_c'}(\eta + S_0)A^* + (\alpha c)^{-1}\frac{\partial A^*}{\partial\bar{x}}\right]Q_{n+1,\eta}.\end{aligned} \tag{B 4}$$

Equation (2.45) can be rewritten as

$$\begin{aligned}\int_{-\infty}^{\infty}\widehat{\Omega}_1\,\mathrm{d}\eta = &\Lambda_1(\partial_\tau - \mathrm{i}S_0)B + \Lambda_2\frac{\partial B}{\partial\bar{x}}\\ &-\frac{\alpha\bar{U}_c'^2}{\bar{U}_c'''}\left[\gamma_{11}A_{\bar{x}\bar{x}} + \gamma_{12}(\partial_\tau - \mathrm{i}S_0)A_{\bar{x}} + \gamma_{22}(\partial_\tau - \mathrm{i}S_0)^2 A\right].\end{aligned} \tag{B 5}$$

It may be deduced using (B 4) that as $\eta \to \pm\infty$,

$$\begin{aligned}\widehat{\Omega}_n \sim &\left\{\frac{\mathrm{i}}{n\eta} - \frac{\mathscr{D}_0}{(n\eta)^2}\right\}(\mathscr{D}_0 - n\mathrm{i}S_0)\,\widehat{b}_2^{(n)} - \delta_{1n}\frac{\mathrm{i}\,(\alpha c)^{-1}}{\eta^2}(\mathscr{D}_0 - \mathrm{i}S_0)\,A_{\bar{x}}\\ &+ \delta_{1n}\left\{\frac{\mathrm{i}}{\eta} - \frac{\mathscr{D}_0}{\eta^2}\right\}\left\{\frac{\mathrm{i}\chi_a}{\alpha\bar{U}_c'}(\mathscr{D}_0 - \mathrm{i}S_0)^2 A + \mathrm{i}\,(\alpha c)^{-1}(\mathscr{D}_0 - \mathrm{i}S_0)A_{\bar{x}}\right\}\\ &- \delta_{2n}\left\{\frac{\mathrm{i}}{2\eta} - \frac{\mathscr{D}_0}{(2\eta)^2}\right\}\left[\frac{1}{2}\frac{\bar{U}_c^{iv}}{\alpha\bar{U}_c'\bar{U}_c'''}(\mathrm{i}A^2)\right] \quad (n \neq 0),\end{aligned} \tag{B 6}$$

$$\widehat{\Omega}_0 \sim \frac{1}{\eta}(\alpha c)^{-1}\mathscr{M}_1 + \frac{1}{\eta^2}\left\{(\alpha c)^{-1}\left[S_0\mathscr{M}_1 + (\mathrm{i}\mathscr{M}_2 + \text{c.c.})\right] - (\widehat{b}_2^{(1)}A^* + \text{c.c.}) + \frac{\bar{U}_c^{iv}}{\alpha\bar{U}_c'\bar{U}_c'''}\left[\mathrm{i}A^*\mathscr{D}_0 A + \text{c.c.} + 2S_0|A|^2\right]\right\} + O(\eta^{-3}), \tag{B 7}$$

where we have put

$$\mathscr{M}_1 = \int_0^\infty \frac{\partial}{\partial\bar{x}}|A(\bar{x}-\xi,\tau-\xi)|^2\,\mathrm{d}\xi, \tag{B 8a}$$

$$\mathscr{M}_2 = \int_0^\infty \left[A_{\bar{x}}^*\mathscr{D}_0 A + A^*\mathscr{D}_0 A_{\bar{x}}\right](\bar{x}-\xi,\tau-\xi)\,\mathrm{d}\xi. \tag{B 8b}$$

In the upstream region ($\bar{x}\to-\infty$), nonlinear terms in (B 4) are negligible. The 'initial condition' satisfied by $\widehat{\Omega}_1$ can be derived as

$$\begin{aligned}\widehat{\Omega}_1 \sim -\int_0^\infty &\left\{(\mathscr{D}_0 - \mathrm{i}S_0)B(\bar{x}-\xi,\tau-\xi) + \frac{\mathrm{i}\chi_a}{\alpha\bar{U}_c'}(\mathscr{D}_0-\mathrm{i}S_0)^2 A(\bar{x}-\xi,\tau-\xi)\right.\\ &\left.+\mathrm{i}(\alpha c)^{-1}(\mathscr{D}_0-\mathrm{i}S_0)\frac{\partial}{\partial\bar{x}}A(\bar{x}-\xi,\tau-\xi)\right\}\mathrm{e}^{-1/3\bar{\lambda}\xi^3-\mathrm{i}\eta\xi}\,\mathrm{d}\xi\\ &+\mathrm{i}(\alpha c)^{-1}\int_0^\infty(\mathscr{D}_0-\mathrm{i}S_0)^2\frac{\partial}{\partial\bar{x}}A(\bar{x}-\xi,\tau-\xi)\xi\mathrm{e}^{-1/3\bar{\lambda}\xi^3-\mathrm{i}\eta\xi}\,\mathrm{d}\xi\\ &+\frac{1}{3}\mathrm{i}(\alpha c)^{-1}\bar{\lambda}\int_0^\infty(\mathscr{D}_0-\mathrm{i}S_0)\frac{\partial}{\partial\bar{x}}A(\bar{x}-\xi,\tau-\xi)\xi^3\mathrm{e}^{-1/3\bar{\lambda}\xi^3-\mathrm{i}\eta\xi}\,\mathrm{d}\xi.\end{aligned} \tag{B 9}$$

Use of this expression in (B 5) leads to

$$\frac{\partial B}{\partial\bar{x}} + c_g^{-1}\frac{\partial B}{\partial\tau} = -\pi\mathrm{i}\left\{\frac{\mathrm{i}\chi_a}{\alpha\bar{U}_c'}(\mathscr{D}_0-\mathrm{i}S_0)^2A + (\alpha c)^{-1}(\mathscr{D}_0-\mathrm{i}S_0)A_{\bar{x}}\right\}\Big/(\Lambda_2+\pi) \tag{B 10}$$

$$+\frac{\alpha\bar{U}_c'^2}{\bar{U}_c'''}\left[\gamma_{11}A_{\bar{x}\bar{x}} + \gamma_{12}(\partial_\tau - \mathrm{i}S_0)A_{\bar{x}} + \gamma_{22}(\partial_\tau-\mathrm{i}S_0)^2A\right]/(\Lambda_2+\pi). \tag{B 10}$$

The solution for B may be written as

$$B = \sum_n B_n \mathrm{e}^{\kappa_0^{(n)}\bar{x}}, \tag{B 11}$$

substitution of which along with (3.24) into (B 10) shows that

$$B_n' = \kappa_0^{(n)}B_n + \kappa_1^{(n)}A_n, \tag{B 12}$$

where

$$\kappa_1^{(n)} = -\pi\mathrm{i}\left\{\frac{\chi_a}{\alpha\bar{U}_c'}\left[\kappa_0^{(n)} - \mathrm{i}(S_0+n\Delta)\right]^2 + (\alpha c)^{-1}\left[\kappa_0^{(n)} - \mathrm{i}(S_0+n\Delta)\right]\kappa_0^{(n)}\right\}\Big/(\Lambda_2+\pi)$$

$$+\frac{\alpha\bar{U}_c'^2}{\bar{U}_c'''}\left\{\gamma_{11}\kappa_0^{(n)2} - \mathrm{i}\gamma_{12}(S_0+n\Delta)\kappa_0^{(n)} - \gamma_{22}(S_0+n\Delta)^2\right\}\Big/(\Lambda_2+\pi). \tag{B 13}$$

Since $A_n = a_0^{(n)}\exp\{\kappa_0^{(n)}\bar{x}\}$, the solution for B_n is

$$B_n = b_0^{(n)}\exp\{\kappa_0^{(n)}\bar{x}\} + \kappa_1^{(n)}a_0^{(n)}\bar{x}\exp\{\kappa_0^{(n)}\bar{x}\}; \tag{B 14}$$

here the constant $b_0^{(n)}$ must be set to zero. The reason for this as well as for the appearance of the factor $\bar{x}$ in B_n transpires if one notes that the amplitude of the instability mode, up to $O(\epsilon^{1/2})$ accuracy, is $A_n + \epsilon^{1/2}B_n$. Thus $b_0^{(n)} \exp\{\kappa_0^{(n)}\bar{x}\}$ may be absorbed into A_n so that the latter is precisely defined. Moreover, during the linear stage upstream, or more precisely for $1 \ll (-\bar{x}) \ll \epsilon^{-1/2}$,

$$A_n + \epsilon^{1/2}B_n = a_0^{(n)} \exp\{(\kappa_0^{(n)} + \epsilon^{1/2}\kappa_1^{(n)})\bar{x}\}, \tag{B 15}$$

which indicates that $\kappa_1^{(n)}$ represents an $O(\epsilon^{1/2})$ correction to the linear growth rate.

REFERENCES

BROWN, G. L. & ROSHKO, A. 1974 On density effects and large structure in turbulent mixing layers. *J. Fluid Mech.* **64**, 775–816.

CHEUNG, L. C. & LELE, S. K. 2009 Linear and nonlinear processes in two-dimensional mixing layer dynamics and sound radiation. *J. Fluid Mech.* **625**, 321–351.

COWLEY, S. J. & WU, X. 1994 Asymptotic approaches to transition modelling. In *Progress in Transition Modelling, AGARD Report* 793, Chapter 3, pp. 1–38.

FREYMUTH, P. 1966 On transition in a separated laminar boundary layer. *J. Fluid Mech.* **25**, 683–704.

GOLDSTEIN, M. E. 1994 Nonlinear interactions between oblique instability waves on nearly parallel shear flows. *Phys. Fluids* A **6**, 724–735.

GOLDSTEIN, M. E. & HULTGREN, L. S. 1988 Nonlinear spatial evolution of an externally excited instability wave in a free shear layer. *J. Fluid Mech.* **197**, 295–330.

GOLDSTEIN, M. E. & LEIB, S. J. 1988 Nonlinear roll-up of externally excited shear layers. *J. Fluid Mech.* **191**, 481–515.

HABERMAN, R. 1972 Critical layers in parallel shear flows. *Stud. Appl. Math.* **51**, 139–161.

HAJJ, M. R. 1997 Stability characteristics of a periodically unsteady mixing layer. *Phys. Fluids* A **9** (2), 392–398.

HERBERT, TH. 1997 Parabolized stability equations. *Annu. Rev. Fluid Mech.* **29**, 245–283.

HO, C. M. & HUERRE, P. 1984 Perturbed free shear layers. *Annu. Rev. Fluid Mech.* **16**, 365–422.

HUERRE, P. & MONKEWITZ, P. A. 1990 Local and global instabilities in spatially developing flows. *Annu. Rev. Fluid Mech.* **22**, 473–537.

HULTGREN, L. S. 1992 Nonlinear spatial equilibration of an externally excited instability wave in a free shear layer. *J. Fluid Mech.* **236**, 635–664.

KACHANOV, Y. S., KOZLOV, V. V. & LEVCHENKO, V. Y. 1979 Experiments on nonlinear interaction of waves in boundary layer. In *IUTAM Symposium on Laminar–Turbulent Transition, Stuttgart, Germany* (ed. E. Eppler & H. Fasel). Springer.

KIM, Y. C., KHADRA, L. & POWERS, E. J. 1980 Wave modulation in a nonlinear dispersive medium. *Phys. Fluids* A **23** (11), 2250–2257.

LEIB, S. J. & GOLDSTEIN, M. E. 1989 Nonlinear interaction between the sinuous and varicose instability modes in a plane wake. *Phys. Fluids* A **1**, 513–521.

LIU, J. T. C. 1989 Coherent structures in transitional and turbulent free shear flows. *Annu. Rev. Fluid Mech.* **21**, 285–315.

MANKBADI, R. R. 1991 Multifrequency excited jets. *Phys. Fluids* **3** (4), 595–605.

MATTINGLY, G. E. & CRIMINALE, W. O. 1972 The stability of an incompressible wake. *J. Fluid Mech.* **51**, 233–272.

MICHALKE, A. 1965 On spatially growing disturbances in an inviscid shear layer. *J. Fluid Mech.* **22**, 371–383.

MIKSAD, R. W. 1972 Experiments on the nonlinear stages of free-shear-layer transition. *J. Fluid Mech.* **56**, 695–719.

MIKSAD, R. W. 1973 Experiments on nonlinear interactions in the transition of a free shear layer. *J. Fluid Mech.* **59**, 1–21.

MIKSAD, R. W., JONES, F. L., POWERS, E. J., KIM, Y. C. & KHADRA, L. 1982 Experiments on the role of amplitude and phase modulations during transition to turbulence. *J. Fluid Mech.* **123**, 1–29.

MIKSAD, R. W., JONES, F. L. & POWERS, E. J. 1983 Measurements of nonlinear interaction during natural transition of a symmetric wake. *Phys. Fluids* **26** (6), 1402–1409.

MOTOHASHI, T. 1979 A higher-order nonlinear interaction among spectral components. *Phys. Fluids* **22** (6), 1212–1213.

RITZ, CH. P., POWERS, E. J., MIKSAD, R. W. & SOLIS, R. S. 1988 Nonlinear spectral dynamics of a transitioning flow. *Phys. Fluids* **31** (12), 3577–3588.

SANDHAM, N. D., MORFEY, C. L. & HU, Z. W. 2006 Nonlinear mechanisms of sound generation in a perturbed parallel jet flow. *J. Fluid Mech.* **565**, 1–23.

SANDHAM, N. D. & SALGADO, A. 1876 Nonlinear interaction model of subsonic jet noise. *Phil. Trans. R. Soc.* **366**, 2745–2760.

SATO, H. 1956 Experimental investigation on the transition of laminar separated layer. *J. Phys. Soc. Japan* **11**, 702–709.

SATO, H. 1959 Further investigation on the transition of two-dimensional separated layer at subsonic speeds. *J. Phys. Soc. Japan* **14**, 1797–1810.

SATO, H. 1970 An experimental study of nonlinear interaction of velocity fluctuations in the transition region of a two-dimensional wake. *J. Fluid Mech.* **44**, 741–765.

SATO, H. & KURIKI, K. 1961 The mechanism of transition in the wake of a thin flat plate placed parallel to a uniform flow. *J. Fluid Mech.* **11**, 321–353.

SATO, H. & SAITO, H. 1975 Fine structure of energy spectra of velocity fluctuations in the transition region of a two-dimensional wake. *J. Fluid Mech.* **67**, 539–559.

SPARKS, C. A. & WU, X. 2008 Nonlinear development of subsonic modes on compressible mixing layers: a unified strongly nonlinear critical-layer theory. *J. Fluid Mech.* **614**, 105–144.

SUPONITSKY, V., SANDHAM, N. D. & MORFEY, C. L. 2010 Linear and nonlinear mechanisms of sound radiation by instability waves in subsonic jets. *J. Fluid Mech.* **658**, 509–538.

STUART, J. T. & DIPRIMA, R. C. 1978 The Eckhaus and Benjamin–Feir resonance mechanisms. *Proc. R. Soc. Lond.* A **362**, 27–41.

WINANT, C. D. & BROWAND, F. K. 1974 Vortex pairing: the mechanism of turbulent mixing-layer growth at moderate Reynolds number. *J. Fluid Mech.* **63**, 237–255.

WU, X. 1996 On an active resonant triad of mixed modes in symmetric shear flows: a plane wake as a paradigm. *J. Fluid Mech.* **317**, 337–368.

WU, X. 2004 Non-equilibrium, nonlinear critical layers in laminar–turbulent transition. *Acta Mechanica Sin.* **20** (4), 327–339.

WU, X. & HUERRE, P. 2009 Low-frequency sound radiated by a nonlinearly modulated wavepacket of helical modes on a subsonic circular jet. *J. Fluid Mech.* **637**, 173–211.